# Combining Variational Modeling with Partial Gradient Perturbation to Prevent Deep Gradient Leakage

Daniel Scheliga, Patrick Mäder, and Marco Seeland *Technische Universität Ilmenau, Germany*
E-mail: {daniel.scheliga, patrick.maeder, marco.seeland}@tu-ilmenau.de

*This work has been submitted to the IEEE for possible publication. Copyright may be transferred without notice, after which this version may no longer be accessible.*

arXiv:2208.04767v1 [cs.LG] 9 Aug 2022

**Abstract**—Exploiting gradient leakage to reconstruct supposedly private training data, gradient inversion attacks are an ubiquitous threat in collaborative learning of neural networks. To prevent gradient leakage without suffering from severe loss in model performance, recent work proposed a *PRivacy EnhanCing mODulE* (PRECODE) based on variational modeling as extension for arbitrary model architectures. In this work, we investigate the effect of PRECODE on gradient inversion attacks to reveal its underlying working principle. We show that variational modeling induces stochasticity on PRECODE's and its subsequent layers' gradients that prevents gradient attacks from convergence. By purposefully omitting those stochastic gradients during attack optimization, we formulate an attack that can disable PRECODE's privacy preserving effects. To ensure privacy preservation against such targeted attacks, we propose *PRECODE with Partial Perturbation* (PPP), as strategic combination of variational modeling and partial gradient perturbation. We conduct an extensive empirical study on four seminal model architectures and two image classification datasets. We find all architectures to be prone to gradient leakage, which can be prevented by PPP. In result, we show that our approach requires less gradient perturbation to effectively preserve privacy without harming model performance.

**Index Terms**—Gradient Leakage, Gradient Inversion, Data Privacy, Federated Learning, Deep Learning, Distributed Machine Learning.

## 1 Introduction

Federated learning leverages the collaborative use of distributed data to boost the performance of neural networks. Multiple clients exchange local training gradients to collaboratively train a common global model, avoiding the need for centrally aggregated or shared data. As training data remains local with each participating client, such collaborative learning systems aim to systematically mitigate privacy risks [1].

However, recent studies demonstrate the reconstruction of potentially sensitive information from the exchanged gradient information, thereby compromising clients' privacy. Particularly advanced in this regard are iterative gradient inversion attacks [2], [3], [4], [5], [6]. Such attacks are based on adjusting initially random dummy data so that the gradient distance between resulting dummy gradients and the attacked victim gradients is minimized.

Perturbation of exchanged gradients is the de-facto standard to defend against such privacy leakage [2], [7], [8], [9], [10], [11], [12]. However, gradient perturbation results in an inherent trade-off between model performance and privacy [2], [4], [8], [13], [14], [15].

To avoid this trade-off, a model-based defense mechanism named *PRivacy EnhanCing mODulE* (PRECODE), was proposed [14]. PRECODE can be used as generic extension for arbitrary model architectures. It utilizes a variational bottleneck to disguise the original latent feature space. The stochasticity induced by variational modeling is supposed to counter iterative gradient inversion attacks by design.

In this work, we investigate the privacy preserving properties of the stochastic sampling within PRECODE in detail. Moreover, we introduce an attack to specifically disable these privacy preserving properties. To also defend against such targeted attacks, we propose a strategic combination of variational modeling and partial gradient perturbation, hence named *PRECODE with Partial Perturbation* (PPP). Extensive experiments on two datasets with four seminal model architectures show that our proposed PPP defense mechanism allows for superior privacy preservation without negative impact on the model performance.

Fig. 1 illustrates a visual summary of the content of this paper. Our contributions can be summarized as follows:

- We analyze model gradients during an iterative gradient inversion attack to reveal how PRECODE counters such attacks by design.
- We show that the privacy preserving properties of PRECODE can only be disabled if attackers explicitly omit gradients affected by PRECODE's stochasticity, loosing relevant information during attack optimization.
- Based on an attackers information loss, we propose PPP as novel defense mechanism, that combines PRECODE's variational modeling with layer specific partial gradient perturbation.
- We perform a systematic empirical evaluation on four seminal model architectures, evaluated on the MNIST and the CIFAR-10 datasets and compare our method with two state of the art defense methods.
- We show that PPP provides a better model performance – privacy trade-off.

The remainder of this work is structured as follows: Section 2 summarizes related work regarding gradient inversion attacks and defense mechanisms. Thereupon we describe the gradient analysis of PRECODE and our attack derived from it. Subsequently,

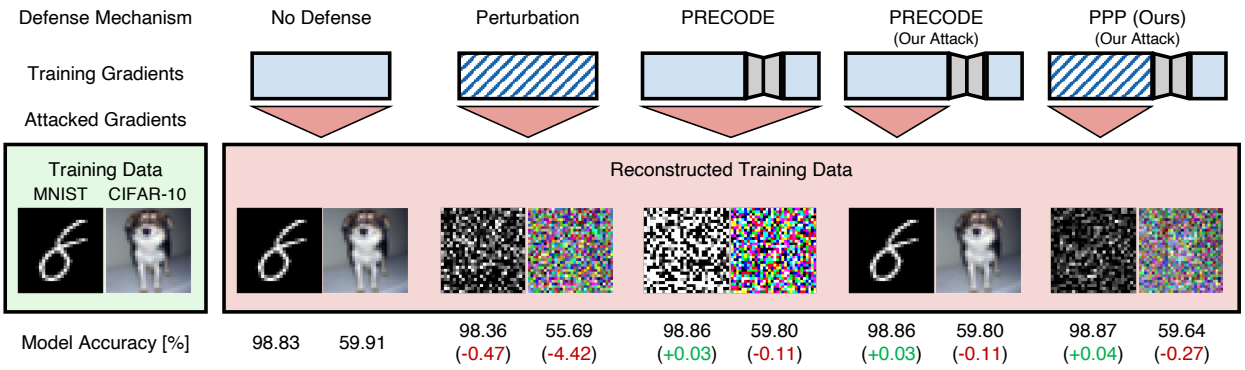


Fig. 1: **Summary of the content of this paper.** Neural networks are trained on the MNIST and CIFAR-10 dataset in a federated scenario. As training gradients leak private training data, different defense mechanism can be used for protection. Training gradients are displayed as blue boxes. Hatched blue-white boxes indicate gradient perturbation whereas grey trapezoids denote defense by a variational bottleneck. Red triangles denote which layers' gradients are used for reconstruction attacks. While state of the art perturbation techniques can prevent reconstruction, they reduce model performance. At first PRECODE seems to defend against gradient leakage while not harming model performance. However, our proposed targeted attack on PRECODE can fully disable its privacy inducing effects. Finally we propose to combine PRECODE with Partial Perturbation (PPP) to prevent reconstruction while having minimal impact on model performance.

we introduce and discuss our proposed PPP defense. Section 4 describes the experimental setup. Experimental results and their discussion are given in Section 5. Finally, we conclude our work and give an outlook on future research.

## 2 Related Work

### 2.1 Gradient Inversion Attacks

Gradient inversion attacks aim to reconstruct training data $(x, y)$ from their corresponding gradients $\nabla\mathcal{L}_\theta(\hat{y}, y)$ [2]. Here $\hat{y} = F(x)$ denotes the prediction of the attacked model $F$ after forward propagation of an input $x$, $y$ the expected output for $x$ and $\mathcal{L}$ the loss function used to optimize the model parameters $\theta$.

We investigate the *honest-but-curious* server scenario [5], which is particularly relevant for collaborative training processes such as *federated learning* [1], [16]. In detail, an attacker has insight into the training process, *i.e.*, knowledge of $\mathcal{L}$, $F$, $\theta$ and $\nabla\mathcal{L}_\theta(\hat{y}, y)$, but does not actively interfere with it (*honesty*). Instead, the attacker aims to reconstruct training data $(x, y)$ of another client participating in the training process (*curiosity*).

In federated learning, training data is not shared but remains local with each client. Clients that participate in the collaborative training process initialize their local model from a global model state. After a defined number of local training steps, clients return their local model updates, *i.e.*, their model gradients, and a new global model state is computed by aggregation of the clients' gradients. This procedure is repeated iteratively until convergence or some other termination criterion is satisfied. Other collaborative training approaches, such as peer-to-peer or cluster-based collaborative training [17], [18], [19] suffer from similar vulnerabilities, as they are based on the exchange of gradient information by design.

Gradient inversion attacks of an *honest-but-curious* attacker can generally be formulated as following optimization problem:

$$\arg\min_{(x',y')} D(\nabla\mathcal{L}_\theta(F(x), y), \nabla\mathcal{L}_\theta(F(x'), y')) + \lambda\Omega. \quad (1)$$

In Eq. 1, a random dummy image $x'$ is fed into the model $F$ of known architecture to obtain a dummy gradient $\nabla\mathcal{L}_\theta(F(x'), y')$, where $y'$ is a randomly initialized dummy label. To reconstruct the original training data $(x, y)$, the distance $D$ between the victim gradient $\nabla\mathcal{L}_\theta(F(x), y)$ and the dummy gradient is iteratively minimized. $\Omega$ describes an additive regularization term which is weighted by $\lambda$. Using gradient based optimization, the dummy data $(x', y')$ is adjusted until convergence.

*Deep Leakage from Gradients* (DLG) [2] first formulates this iterative gradient inversion attack using Euclidean distance for $D$, no regularization term and a L-BFGS optimizer [20]. Zhao *et al.* improve DLG (iDLG) [3] by analytically reconstructing the ground-truth labels $y$ in advance. It has been found that omitting the necessity of optimizing for $y'$ in Eq. 1 accelerates and stabilizes the optimization process. Although iDLG only guarantees to reconstruct the labels for batches of size 1, the authors of [6] formulate a method to reliably reconstruct label information of arbitrarily large batches that contain disjoint classes.

The *inverting gradient attack* (IGA) [5] further improves the reconstruction process by disentangling gradient direction and magnitude. In Eq. 1, the cosine distance between victim and dummy gradients is minimized instead of the Euclidean distance. Furthermore, they use total variation [21] of the dummy image $x'$ as regularization to constrain the reconstruction to relevant image parts. Additionally, the Adam optimizer [22] was found to generally yield more sophisticated reconstruction results compared to L-BFGS. Further work on improving the quality of iterative gradient inversion attacks mainly focuses on the choice of the 1) gradient distance function $D$, 2) regularization term $\Omega$, 3) optimizer and 4) label reconstruction method [4], [6], [23], [24], [25]. An elaborate overview of combinations for recent attacks can be found in [26].

### 2.2 Defense Mechanisms

The authors of [4] present a comprehensive analysis of gradient inversion attacks and deduce relevant parameters as well as potential mitigation strategies. They found that batch size, image resolution, choice of activation functions and the number of local

training epochs can impact privacy leakage. Supporting findings are reported in [2], [3], [5], [27], [28]. Furthermore, the training progress was found to impact privacy leakage from gradients since models trained for more communication rounds typically yield smaller gradients compared to early stages of the overall training [5], [14], [23].

However, even if training parameters are carefully selected to prevent gradient inversion attacks, there is no guarantee that reconstruction of sensitive data is not possible [5]. As a matter of fact, Geiping *et al*. showcased successful attacks on deep neural networks (ResNet-152) trained for multiple communication rounds and even for batches of 100 images [5]. Additionally, parameter selection is often controlled by other factors, like model and/or hardware limitations. Therefore, to achieve data privacy, defense mechanisms should be actively developed, analyzed and applied.

#### 2.2.1 Cryptography-based Defense

Although cryptographic methods such as secure aggregation schemes [7], [29] and homomorphic encryption [30], [31] are likely to provide the best privacy preservation, they come at extreme computational costs and are not applicable in every collaborative learning scenario. For example Pasquini *et al*. [32] demonstrate that for particular federated learning scenarios, secure multiparty computation schemes can be practically bypassed, allowing for gradient inversion attacks as described above.

Instead of using costly cryptographic methods, the de-facto standard to defend against privacy leakage is perturbation of exchanged gradients.

#### 2.2.2 Gradient Perturbation

Typically three approaches are utilized for gradient perturbation: *gradient quantization*, *gradient compression*, and *noisy gradients*. *Gradient quantization* primarily aims to reduce communication costs and memory consumption during collaborative training [10], [16]. Fixed ranges of numerical values are compressed to sets of values, reducing the entropy of the quantized gradients. As a side effect, this also reduces the success of gradient inversion attacks. The authors of [2] found only low-bit Int-8 quantization to be sufficient for defending against inversion attacks. However, this caused a $22.6\%$ drop in model accuracy [2], which is not acceptable in practical scenarios.

*Gradient compression* or *sparsification* by pruning is another method introduced to reduce the communication costs during collaborative training [33], [34]. For each layer of the model the gradient elements that carry the least information, *i.e*., have the smallest magnitude, are pruned to zero. Similar to quantization, this decreases reconstruction success by inversion attacks since the entropy of the gradient is reduced [2], [4], [15].

The use of noise to limit information disclosure about individuals is an approach originally introduced in the field of differential privacy [1], [13], [35]. To guarantee a provable degree of privacy to clients participating in collaborative training, state of the art methods use *noisy gradients* [7], [36], [37]. Naive approaches simply add Gaussian or Laplace noise to the gradients prior to their exchange, while more sophisticated approaches use a combination of quantization or gradient clipping and a carefully tuned noise injection [11], [12]. For example Wei *et al*. adaptively add more noise if the gradients have high entropy early in training and less noise when the gradients carry less information for reconstruction later in training [12].

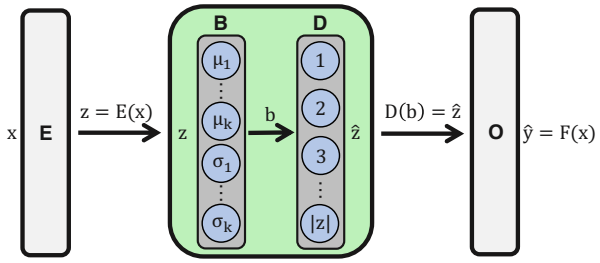


Fig. 2: Realization of the PRECODE extension as variational bottleneck. Reprinted with permission from [14] (©[2022] IEEE)

A major advantage of differentially private algorithms are the *theoretical guarantees* on how much privacy a model may leak. However, Papernot *et al*. show that the amount of privacy that can be guaranteed decreases with the number of training epochs and number of shared parameters [9]. Although the addition of noise may suppress gradient inversion attacks, it also negatively affects the training process and final model performance. Depending on the level of added noise Wei *et al*. demonstrate that in order to protect the exchanged data from privacy leakage, model accuracy drops of up to $9.8\%$ must be taken into account [4]. Increasing the amount of training data might mitigate such drops in performance [13]. However, this is typically not feasible in practical scenarios.

#### 2.2.3 Model Extension

As discussed above, gradient perturbation is the de-facto standard for defending against gradient leakage. However, gradient perturbation is inherently limited by a well observed trade-off between model performance and privacy [2], [4], [8], [13], [14], [15].

Instead, the authors of [14] propose to extend neural network architectures with a *PRivacy EnhanCing mODulE* (PRECODE) that aims to prevent privacy leakage by gradient inversion attacks. The module can be generically integrated into any existing model architecture without requiring further model modifications. More importantly, the module does not notably harm the final model performance or training process, *e.g*., by causing increased convergence times.

PRECODE is implemented as a variational bottleneck (VB), which originates from the field of generative modeling. VBs aim to learn a joint distribution between the input data in its latent representation [38]. As visualized by Figure 2, they consist of a probabilistic encoder $B = q(b|z)$ and decoder $D = p(z|b)$. The VB approximates the distribution of the latent space and obtains new representations $\hat{z}$ from an approximated prior distribution $p(b)$ by stochastic sampling from a multivariate Gaussian.

The bottleneck $B$ is realized as a fully connected layer with $2k$ neurons, where $k$ defines the size of the bottleneck representation $b$. $z = E(x)$ represents the latent representations computed by forward propagation of an input sample $x$ through all layers $E$ of the base neural network prior to the output layer. The bottleneck $B$ encodes this representation $z$ into a latent distribution which fits a multivariate Gaussian:

$$B(z) = q(b|z) = \mathcal{N}(\mu_B, \sigma_B) \tag{2}$$

where $[\mu_B, \sigma_B] = [\mu_1, \mu_2, \ldots, \mu_k, \sigma_1, \sigma_2, \ldots, \sigma_k]$ are described by the bottleneck neurons.

The bottleneck features $b \sim q(b|z)$ are then fed into the stochastic decoder $D$, which is also realized as a fully connected

layer. The number of neurons in $D$ matches the number of features in $z$. $D$ computes a new latent $\hat{z} = p(z|b)p(b)$ which is then used to calculate the model prediction $\hat{y} = O(\hat{z})$, where $O$ corresponds to the layer(s) of the neural network that follow the VB.

The loss function $\mathcal{L}_F$ of the base model $F$ is extended by the Kullback-Leibler divergence ($D_{KL}$) between $\mathcal{N}(\mu_B, \sigma_B)$ and a standard normal distribution, so that the VB learns a complete and continuous latent feature space distribution:

$$\mathcal{L}(\hat{y}, y) = \mathcal{L}_F(\hat{y}, y) + \beta \cdot D_{KL}(\mathcal{N}(\mu_B, \sigma_B), \mathcal{N}(0, 1)). \quad (3)$$

$\beta$ controls the weight of the VB loss on the overall loss function. In order to backpropagate a gradient through the bottleneck layer, the reparameterization technique described in [38] is used. PRECODE is by default inserted between the last feature extracting layer and the final classification layer of a given base neural network. We based our experiments on the provided PyTorch implementation of PRECODE[1].

## 3 Decoding PRECODE

The VB realizes a *stochastic function* which transforms input representations $z$ to stochastic latent representations $\hat{z}$. As $\hat{y}$ and $\mathcal{L}(\hat{y}, y)$ are computed based on this stochastic representation, the gradient $\nabla\mathcal{L}(\hat{y}, y)$ does not contain direct information on the input sample $x$. Furthermore, iterative optimization-based attacks are countered by design, since $\hat{z}' = E(x')$ is sampled randomly in each optimization step of the attack. Small changes in $x'$ cause an increased entropy of $\hat{z}'$, making it difficult for the optimizer to find dummy images $x'$ that minimize the reconstruction loss.

### 3.1 The Impact of Bias Weights

Recent work shows that the input to any fully connected layer in a neural network can be analytically reconstructed [5], [39]. As PRECODE consists of fully connected layers, there is no need for iterative gradient inversion attacks to 1) reconstruct the feature maps that are input to PRECODE and 2) to fully reconstruct training data from MLPs protected with PRECODE [40]. However, removing the bias weights from all fully connected layers can easily mitigate analytical attacks without harming model performance. In turn, this makes iterative gradient inversion attacks the biggest threat for privacy leakage from gradients. More details and experimental results can be found in the *Supplementary Material*.

### 3.2 Gradient Analysis

To analyze the impact of PRECODE on the models' gradients during an iterative gradient inversion attack, we tracked the evolution of dummy gradients of the last layer of the network for each iteration step during the attack, *i.e.*, for each update of a dummy image. The same was done for the model without PRECODE. To realize the easiest scenario for an attacker, we used a Multi Layer Perceptron (MLP), a single random image from the CIFAR-10 dataset and IGA as gradient inversion attack. The MLP had four hidden layers of size 1024, batch normalization and ReLU activation. The last layer of the MLP had ten neurons with softmax activation. We repeated this analysis for different model inputs and observed similar behaviour.

In Figure 3(a) the change of two randomly chosen dummy gradient values $g'_1$ and $g'_2$ of the model's output layer is illustrated for both the MLP and its variant protected by PRECODE. The iteration progress is represented by change in color. For the unprotected baseline model the dummy gradient values converge to the corresponding victim gradient values after only a few attack iterations. This indicates that the dummy image quickly converges to an image that leads to the same gradient as the original training data.

The random sampling process in the PRECODE bottleneck causes the latent representation of the dummy image $\hat{z}'$ to take new values in each attack iteration. Even if the same dummy image is forwarded through the network, the random sampling in the PRECODE bottleneck would result in different gradients. In result, if the dummy gradient points into a different direction at every attack iteration, the optimizer of the iterative gradient inversion attack cannot find a consistent direction to minimize the distance between the victim and the dummy gradient.

Figures 3(b-c) further illustrate this behaviour in an aggregated manner. The norms of the dummy gradients in Figure 3(b) for all layers of the baseline MLP become consistently more stable over the course of the attack as the dummy images and their gradients converge towards the original ones. This is also reflected by the increasing cosine similarity between the dummy and victim gradients in Figure 3(c).

Because of the adapted loss function as described in Eq. 3, the gradient values of the PRECODE decoder and the last classification layer differ by almost one order of magnitude compared to the other layers. During attack optimization, the distance loss between victim and dummy gradients is mainly influenced by gradients with large norm, *i.e.*, gradients that result from stochastic sampling. As the gradient direction for those layers change in each attack iteration (cf. Figure 3(a)) the optimization process cannot converge. In result, the cosine similarity of the gradients of the PRECODE decoder and the final classification layer are fluctuating on a low similarity level. The higher the gradient norms of the other layers are, the higher is their influence on the gradient distance and change of the dummy image. Accordingly, the cosine similarities are lower for earlier layers. For the first layer they even remain constant near zero.

### 3.3 Attacking PRECODE

Inspired by [40] we leverage the idea of purposefully ignoring specific parts of a defense mechanism in order to disable the protection induced by PRECODE. Based on the findings of our gradient analysis, we propose to remove the high influence of the stochastic gradients on the attack optimization. Given the gradients $\nabla\mathcal{L}_\theta(F(x), y) = G = [G_1, \ldots, G_B, G_D, \ldots, G_n]$ we omit $[G_B, G_D, \ldots, G_n]$, *i.e.* PRECODE's and its subsequent layers gradients, during the optimization of the dummy data. Indices $i$ of $G_i$ denote the layers position and $G_B$ and $G_D$ denote PRECODE's bottleneck and decoder layer. Correspondingly $\nabla\mathcal{L}_\theta(F(x'), y') = G'$ refers to the dummy gradient. Hence the reconstruction loss for the inversion attack is only calculated through the distance $D$ between the victim and dummy gradients layers $[G_1, \ldots, G_{B-1}]$, that precede the PRECODE variational bottleneck:

$$D([G_1, \ldots, G_{B-1}], [G'_1, \ldots, G'_{B-1}]) \quad (4)$$

The adjustments on the dummy image would stabilize as they are based only on the more stable dummy gradients. Hence, the dummy data could converge towards the actual input data. We empirically confirm this hypothesis in Section 5.1.

1. https://github.com/dAI-SY-Group/PRECODE

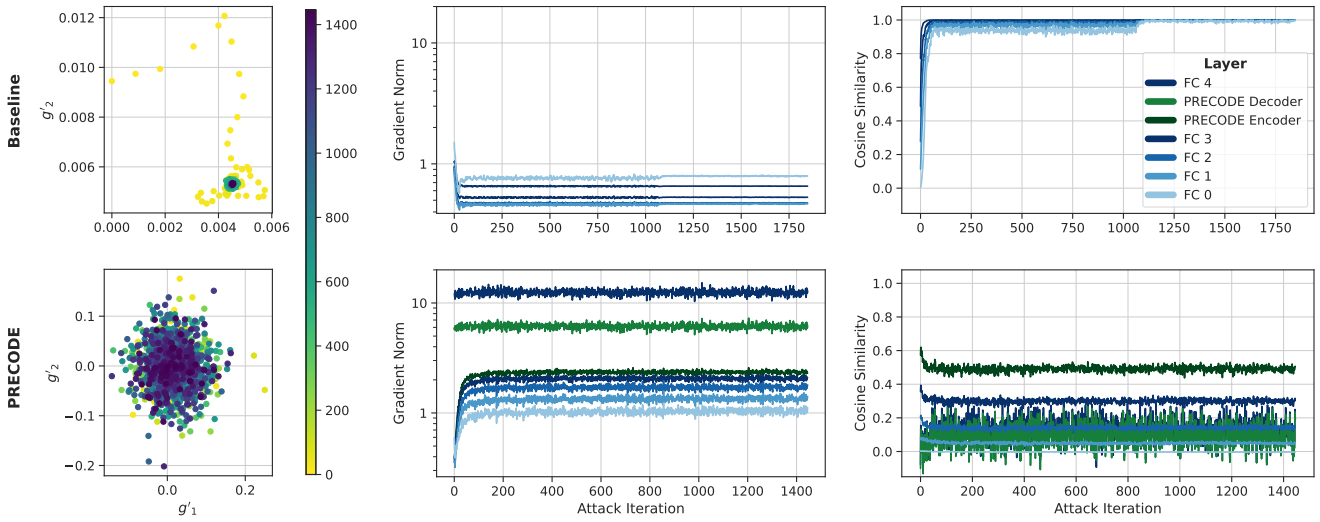


(a) (b) (c)

Fig. 3: **Behaviour of dummy gradients during a gradient inversion attack** for a MLP (top) and a MLP that is protected by PRECODE (bottom). (a) Two random gradient values $g'_1$ and $g'_2$ of dummy gradients $G'$ of the last layer are tracked over the course of the inversion attack. Color represents the attack iteration. (b) Gradient norms of dummy gradients and (c) cosine similarities between dummy gradients and the victim gradient for each model layer over the course of the inversion attack. Color represents the layer of the model, whereas MLPs layer use blue shades and the PRECODE VB layers use green ones.

### 3.4 PRECODE with Partial Perturbation (PPP)

Our proposed attack reveals that PRECODE is vulnerable to more sophisticated attacks. In order to prevent gradient leakage and preserve privacy, we propose to combine *PRECODE with Partial gradient Perturbation*, hereafter denoted as PPP. Using gradient perturbation, high levels of noise are required for protecting models from gradient leakage. Typically, this has a notable negative impact on the model performance [2], [4], [8], [13], [14], [15]. We argue that the combination of PRECODE and gradient perturbation is less harmful to the model performance, as only layers preceding PRECODE require protection by gradient perturbation. All subsequent layers are entirely protected by PRECODE (cf. Section 3.2). Hence, we propose to perturb the gradients $[G_1, \ldots, G_{B-1}]$ of all layers from the input of the model to PRECODE's variational bottleneck. Details on the choice of perturbation and perturbation level are discussed in Section 5.2.

## 4 Experimental Setup

This section describes the experimental settings used to conduct systematic empirical studies that evaluate model performance and privacy leakage for different datasets, model architectures, and defense mechanisms.

### 4.1 Model Performance

To measure the impact of different defense mechanisms on the model performance, models are trained for image classification on MNIST [41] and CIFAR-10 [42]. Both datasets are first separated into training and test splits according to the corresponding benchmark protocols. We embedded all experiments in a federated learning scenario with 10 clients. The training data splits are therefore evenly distributed to those 10 clients, leaving each client with $6'000$ and $5'000$ training samples for MNIST and CIFAR-10 respectively. The clients collaboratively train a randomly initialized model for 200 communication rounds. In each communication round, (1) a central aggregator transmits the current global model state, (2) each client trains a local model based on the transmitted global model state and the private local training data for 1 epoch, and (3) aggregation of model gradients from all clients and computation of an updated global model state by the central aggregator. Local training minimizes the cross-entropy loss using Adam optimizer [22] with learning rate $0.001$, momentum parameters $\beta_1 = 0.9$ and $\beta_2 = 0.999$, and a batch size of 64.

When using PRECODE, each architecture is extended by a VB with $k = 256$ and $\beta = 0.001$. According to the findings in [14], the VB is placed between the last feature extracting layer and the final classification layer of the model. The loss function is adjusted according to Eq. 3.

When using gradient perturbation techniques as defense mechanism, local model gradients of the clients are perturbed before transmission to the central aggregator. In terms of model performance, accuracy of the global model states is evaluated on the test data after every communication round. We repeated each experiment and report the average across three runs using different random seeds.

### 4.2 Privacy

To evaluate privacy leakage, a *victim dataset* composed of 128 images is randomly sampled from the training data of one client for each dataset. A victim gradient is then computed by performing a single training step using that victim data. To ease reconstruction for the attacker, each victim image is attacked independently. As gradient inversion attack, we use the publicly available PyTorch implementation of IGA[2] provided by [5]. We configured the attack as follows: dummy images are initialized from Gaussian distribution, cosine distance is used as loss function, and total variation as regularization term with weight $\lambda = 0.01$. For each

2. https://github.com/JonasGeiping/invertinggradients

TABLE 1: Model performance and privacy metrics for a MLP trained on MNIST and CIFAR-10. Gradients are attacked without any defense (Baseline) and with PRECODE. Arrows indicate direction of improvement. Bold and italic formatting highlight best and worst results respectively. The * denotes that the gradients of all layers are attacked.

| Dataset | Metric / Defense | Accuracy [%] ↑ | SSIM ↓ | PSNR ↓ | MSE ↑ | LPIPS ↑ |
|---|---|---|---|---|---|---|
| MNIST | Baseline* | *98.83* | *1.00* | *60.09* | *0.00* | *0.00* |
| | PRECODE* | **98.86** | **0.01** | **3.52** | **4.68** | **0.71** |
| | PRECODE | | *1.00* | 48.02 | *0.00* | *0.00* |
| CIFAR-10 | Baseline* | **59.91** | *1.00* | *59.50* | *0.00* | *0.00* |
| | PRECODE* | *59.80* | **0.01** | **5.50** | **4.63** | **0.69** |
| | PRECODE | | *1.00* | 49.52 | *0.00* | *0.00* |

attack, Adam optimizer with initial learning rate $0.1$ is used. The learning rate is reduced by a factor of $0.1$ if the reconstruction loss plateaus for $800$ attack iterations. To save computational resources, attacks are stopped if either the reconstruction loss falls below a value of $10^{-5}$, or there is no decrease in reconstruction loss for $4'000$ iterations, or after a maximum of $20'000$ iterations.

To ease reconstruction, we assume label information to be generally known for each attacked sample. Please note that label information can be analytically reconstructed from gradients of cross-entropy loss functions w.r.t. weights of fully connected layers with softmax activation [3], [4], [5]. This analytical reconstruction of label information might be hindered by the adjusted loss function when using PRECODE. However, to avoid systematic advantage of PRECODE and PPP, we assume label information to be generally known irrespective of the defense mechanism.

Similar to [26], we compute *Mean Squared Error* (MSE), *Peak Signal-to-Noise Ratio* (PSNR), *Structural Similarity* (SSIM) [43], and a *Learned Perceptual Image Patch Similarity* (LPIPS) [44] between original and reconstructed images to measure the reconstruction quality. Privacy leakage correlates with higher reconstruction quality and is indicated by lower MSE and LPIPS as well as higher PSNR and SSIM values. All reported metrics are averaged across the respective $128$ samples of each victim dataset.

## 5 Experimental Results and Discussion

### 5.1 Attacking PRECODE

In this first set of experiments we attack a MLP protected with PRECODE as described in Section 3.3. As can be seen in Table 1, the baseline models without any protection are vulnerable to gradient inversion attacks and allow for perfect reconstruction of training data. Extending the models by PRECODE extensively protects against usual gradient inversion attacks, *i.e.*, the reconstruction quality collapses as measured by reducing SSIM and PSNR and increasing MSE and LPIPS.

However, if PRECODE is attacked by purposefully ignoring the gradients of PRECODE and its subsequent layers, the attacker is able to fully reconstruct the original training data. Excluding the stochastic gradients from attack optimization fully disables PRECODE's intended privacy inducing effects. However, we observed that the number of iterations and therefore the computational power needed for reconstruction is more than tripled since less gradient information is usable for the attack. On average, the number of iterations needed for reconstruction increased by a factor of $3.26$ for the CIFAR-10 victim data and $4.74$ for the MNIST victim data. More detailed experimental results can be found in the *Supplementary Material*. Hence, although PRECODE cannot protect the privacy of training data, the computational difficulty of the attacks is notably increased.

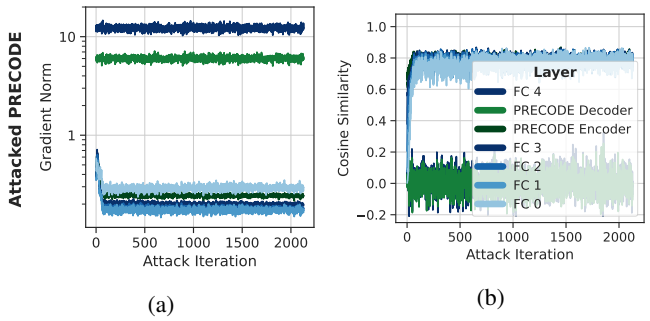


(a) (b)

Fig. 4: **Behaviour of dummy gradients during a gradient inversion attack** for a PRECODE protected MLP, where PRECODE is attacked as described in Section 3.3. Cosine similarities (a) between dummy gradients and the victim gradient and gradient norms (b) of dummy gradients are tracked over the course of the inversion attack. Color represents the layer of the model, whereas MLPs layer use blue shades and the PRECODE VB layers use green ones.

Analogous to the gradient analysis in Section 3.2, Figure 4 shows the behaviour of the dummy gradients of the model with attacked PRECODE over the course of the inversion attack. As suspected, the gradient norms of the first layers start to decrease similarly to attacking the baseline model. Gradient norms and cosine similarities of the PRECODE decoder and final layer also behave similar, however, they do not impact the optimization process anymore. Since only stable dummy gradients influence the attack optimization, the dummy data adapts towards the original data. This can be observed in terms of converging cosine similarity (cf. Figure 4(b)) between the dummy and the victim gradients for layers that precede PRECODE. However, backpropagation through the VB still increases the variance of the dummy gradients. In result, whereas the attack optimization of the baseline model quickly converged and achieved dummy gradients with cosine similarities close to $1$ (cf. Figure 3(b)), the dummy gradients with PRECODE protection only achieve similarities close to $0.8$ (cf. Figure 4(b)).

### 5.2 Combining PRECODE with Partial Perturbation

As motivated in Section 3.4 we propose a strategic combination of PRECODE with Partial gradient Perturbation to defend against more sophisticating attacks. In all experiments utilizing PPP defense, we used our proposed attack as described in Section 3.3. First, we evaluate our proposed approach using MLPs as these are most vulnerable to gradient leakage.

For comparative evaluation, we also defend against inversion attacks using gradient perturbation techniques on entire gradients. We consider noisy gradients [45] (NG) and gradient compression [33] (GC), each with different perturbation levels. Gradient quantization is not considered due to the comparatively large negative impact on model performance [2]. For NG, we add noise sampled from Gaussian distribution with zero mean and standard deviation $\sigma$. We use increasing of noise levels by setting $\sigma \in [10^{-3}, 10^{-2}, 10^{-1}, 5 \cdot 10^{-1}]$, denoted in the experiments as [NG3, NG2, NG1, NG05].

For GC the gradient values with smallest magnitudes are pruned to zero for every gradient layer, as described in [15].

TABLE 2: Mean model performance and privacy metrics for a MLP trained on MNIST and CIFAR-10. The gradients are attacked for different defense mechanisms. When PRECODE or PPP is used, our proposed targeted attack is applied. Arrows indicate direction of improvement. Bold and italic formatting highlight best and worst results respectively.

| Dataset | Metric / Defense | Accuracy [%] ↑ | SSIM ↓ | PSNR ↓ | MSE ↑ | LPIPS ↑ |
|---|---|---|---|---|---|---|
| MNIST | Baseline | 98.83 | *1.00* | *60.09* | *0.00* | *0.00* |
| | NG3 | 98.83 | *1.00* | 42.41 | *0.00* | 0.01 |
| | NG2 | 98.82 | 0.87 | 22.29 | 0.06 | 0.20 |
| | NG1 | 98.36 | 0.11 | 7.43 | 1.91 | 0.67 |
| | NG05 | 93.32 | 0.02 | **6.02** | **2.64** | **0.69** |
| | GC90 | 95.02 | 0.94 | 27.57 | 0.02 | 0.11 |
| | GC99 | *64.93* | 0.72 | 15.98 | 0.30 | 0.35 |
| | PRECODE | 98.86 | *1.00* | 48.02 | *0.00* | *0.00* |
| | $PPP_{NG3}$ | **98.89** | 0.97 | 32.32 | 0.01 | 0.05 |
| | $PPP_{NG2}$ | 98.87 | 0.47 | 12.30 | 0.61 | 0.56 |
| | $PPP_{NG1}$ | 98.40 | 0.03 | 7.20 | 2.01 | 0.68 |
| | $PPP_{NG05}$ | 95.36 | **0.01** | 6.92 | 2.15 | 0.68 |
| | $PPP_{GC90}$ | 98.79 | 0.94 | 27.01 | 0.02 | 0.12 |
| | $PPP_{GC99}$ | 88.90 | 0.78 | 17.24 | 0.20 | 0.35 |
| CIFAR-10 | Baseline | 59.91 | *1.00* | *59.50* | *0.00* | *0.00* |
| | NG3 | **60.08** | 0.99 | 38.65 | *0.00* | 0.01 |
| | NG2 | 59.81 | 0.63 | 18.73 | 0.16 | 0.32 |
| | NG1 | 55.69 | 0.04 | 8.43 | 2.31 | **0.67** |
| | NG05 | *25.55* | **0.01** | **7.80** | **2.69** | **0.67** |
| | GC90 | 55.31 | 0.87 | 23.52 | 0.06 | 0.11 |
| | GC99 | 42.14 | 0.43 | 14.45 | 0.62 | 0.40 |
| | PRECODE | 59.80 | *1.00* | 49.52 | *0.00* | *0.00* |
| | $PPP_{NG3}$ | 59.76 | 0.92 | 28.26 | 0.02 | 0.06 |
| | $PPP_{NG2}$ | 59.64 | 0.17 | 11.39 | 1.12 | 0.60 |
| | $PPP_{NG1}$ | 56.51 | 0.02 | 8.57 | 2.23 | **0.67** |
| | $PPP_{NG05}$ | 48.99 | **0.01** | 8.44 | 2.31 | **0.67** |
| | $PPP_{GC90}$ | 50.92 | 0.87 | 23.73 | 0.06 | 0.11 |
| | $PPP_{GC99}$ | 38.02 | 0.47 | 15.85 | 0.40 | 0.40 |

The amount of pruned values is determined by the pruning ratio $p$, which we choose as $90\%$ (GC90) and $99\%$ (GC99). The experimental results determined by our approach are identified with $PPP_{Pert}$. In all $PPP_{Pert}$ experiments, Pert $\in$ [NG3, NG2, NG1, NG05, GC90, GC99] is applied to the gradients of all layers preceding PRECODE as described in Section 3.4.

Table 2 displays the results with respect to achieved model performance and privacy for both the MNIST and CIFAR-10 datasets. A first observation is that increasing the level of gradient perturbation causes a decrease in model performance, as measured by test accuracy. In addition, high noise levels of $\sigma = 10^{-1}$ (NG1) are required to achieve sufficient protection against gradient leakage. Sufficient privacy protection is achieved if SSIM drops below $0.4$.

Using GC, even a large pruning ratio of 99% does not suffice to protect from gradient leakage. Instead, the model performance is severely reduced. We attribute the insufficient protection of GC to the underlying pruning mechanism: for GC, the smallest elements of layers' gradients are pruned to zero (cf. Section 5.2). On the contrary, gradient inversion is dominated by large valued gradient elements. In result, GC barely impacts gradient inversion attacks unless majority of each gradient is pruned. As such large pruning ratios render the models practically useless, we conclude that GC is generally unsuitable for protection against gradient leakage.

Fig.5 displays example reconstructions for the attacked MLPs for both datasets. As MNIST contains overall less information compared to CIFAR-10, all attacks achieve better reconstructions and require a higher amount of perturbation to protect privacy. The images exemplary confirm the aggregated metrics reported in Table 2: a noise level of $\sigma = 10^{-1}$ (NG1) is required to sufficiently prevent reconstruction, whereas GC seems to suppress comparably irrelevant image regions.

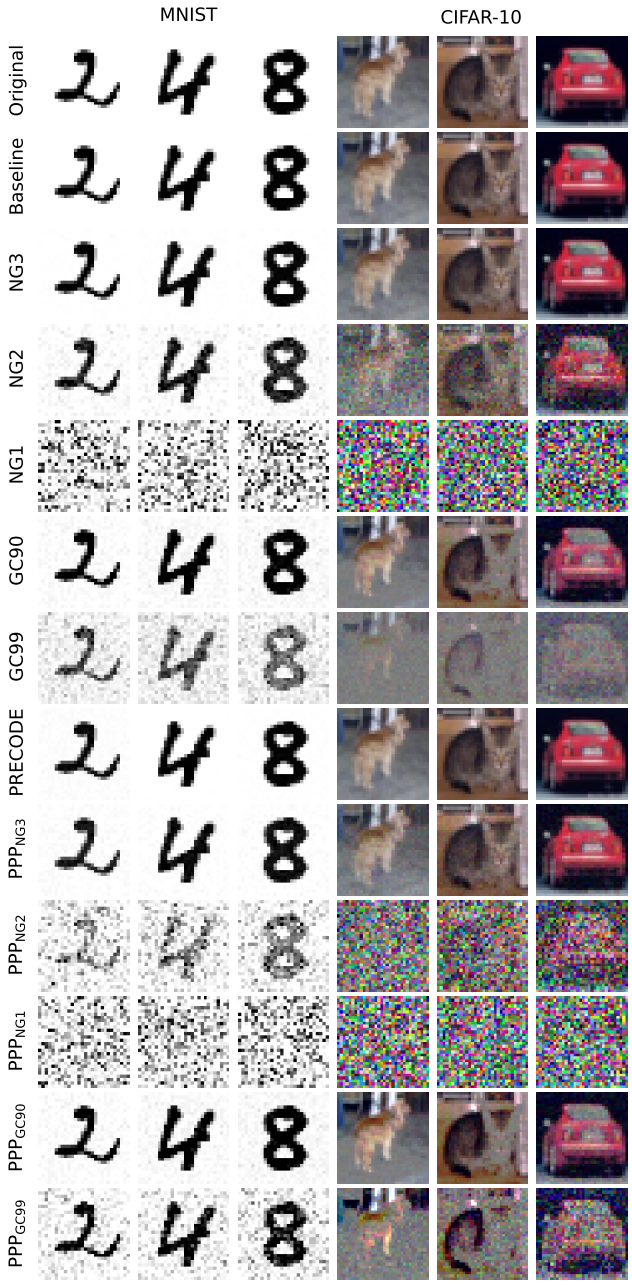


Fig. 5: **Example reconstructions** for the MLP architecture with different defenses on the MNIST and CIFAR-10 datasets.

When using our proposed PPP we observe that less perturbation is required for protection against gradient leakage, confirming the hypothesis made in Section 3.4. In detail, for MNIST and CIFAR-10, $PPP_{NG2}$ and $PPP_{NG1}$ sufficiently protect against gradient leakage. At the same time, this combination barely impacts the model performance.

Confirming the finding using solely GC as defense, also the combination $PPP_{GC}$ does not sufficiently protect from gradient leakage but instead results in a severe drop of model performance.

### 5.3 Other Model Architectures

PRECODE is claimed to be a generic module for arbitrary model architectures [14]. Here, we investigate the efficacy of PRECODE

TABLE 3: Mean model performance and privacy metrics for a LeNet, ResNet and Vision Transformer (ViT) trained on MNIST and CIFAR-10. The gradients are attacked for different defense mechanisms. When PRECODE or PPP is used, our proposed targeted attack is applied. Arrows indicate direction of improvement. Bold and italic formatting highlight best and worst results respectively.

| Dataset | Model | Metric / Defense | Accuracy [%] ↑ | SSIM ↓ | PSNR ↓ | MSE ↑ | LPIPS ↑ |
|---|---|---|---|---|---|---|---|
| MNIST | LeNet | Baseline | 98.89 | 0.99 | 34.47 | *0.00* | 0.01 |
| | | NG3 | **98.90** | *1.00* | *50.05* | *0.00* | *0.00* |
| | | NG2 | 98.81 | 0.98 | 33.38 | 0.01 | 0.04 |
| | | NG1 | *98.19* | 0.70 | 14.18 | 0.51 | 0.39 |
| | | PRECODE | 98.74 | 0.36 | 8.64 | 1.48 | 0.59 |
| | | $PPP_{NG3}$ | 98.68 | 0.35 | 8.57 | 1.54 | 0.59 |
| | | $PPP_{NG2}$ | 98.69 | 0.36 | 8.67 | 1.50 | 0.59 |
| | | $PPP_{NG1}$ | 98.27 | **0.18** | **6.37** | **2.46** | **0.66** |
| | ResNet | Baseline | 99.62 | *0.82* | *18.24* | *0.19* | *0.23* |
| | | NG3 | 99.62 | 0.81 | 18.06 | 0.20 | *0.23* |
| | | NG2 | **99.63** | 0.79 | 17.55 | 0.22 | 0.25 |
| | | NG1 | 99.45 | 0.35 | 11.17 | 0.84 | 0.50 |
| | | PRECODE | 99.58 | 0.22 | **7.40** | **2.16** | 0.57 |
| | | $PPP_{NG3}$ | 99.60 | 0.24 | 7.58 | 2.10 | 0.57 |
| | | $PPP_{NG2}$ | 99.59 | 0.22 | 7.42 | 2.09 | **0.58** |
| | | $PPP_{NG1}$ | *99.43* | **0.08** | 8.01 | 1.73 | **0.58** |
| | ViT | Baseline | 98.70 | 0.99 | 33.35 | 0.01 | 0.01 |
| | | NG3 | 98.69 | *1.00* | *39.73* | *0.00* | *0.00* |
| | | NG2 | 98.72 | 0.84 | 20.55 | 0.11 | 0.16 |
| | | NG1 | *97.21* | 0.15 | 8.93 | 1.40 | 0.56 |
| | | PRECODE | 98.85 | 0.55 | 14.00 | 0.45 | 0.35 |
| | | $PPP_{NG3}$ | **98.86** | 0.54 | 13.93 | 0.46 | 0.35 |
| | | $PPP_{NG2}$ | 98.78 | 0.36 | 11.40 | 0.80 | 0.46 |
| | | $PPP_{NG1}$ | *97.21* | **0.05** | **7.18** | **2.05** | **0.63** |
| CIFAR-10 | LeNet | Baseline | 58.24 | *0.53* | *15.61* | *0.47* | *0.42* |
| | | NG3 | 58.36 | 0.50 | 15.14 | 0.62 | 0.44 |
| | | NG2 | **58.42** | 0.48 | 14.87 | 0.69 | 0.44 |
| | | NG1 | *50.74* | 0.19 | 9.55 | 1.85 | 0.61 |
| | | PRECODE | 56.76 | 0.18 | 9.63 | 1.76 | 0.61 |
| | | $PPP_{NG3}$ | 56.98 | 0.19 | 9.67 | 1.75 | 0.61 |
| | | $PPP_{NG2}$ | 57.48 | 0.17 | 9.42 | 1.87 | 0.61 |
| | | $PPP_{NG1}$ | 53.64 | **0.06** | **7.74** | **2.74** | **0.66** |
| | ResNet | Baseline | **79.46** | *0.56* | *16.27* | 0.35 | *0.39* |
| | | NG3 | 79.20 | *0.56* | 16.19 | *0.34* | *0.39* |
| | | NG2 | 79.19 | 0.54 | 15.95 | 0.36 | 0.40 |
| | | NG1 | *70.55* | 0.16 | 11.71 | 1.03 | 0.58 |
| | | PRECODE | 79.21 | 0.16 | 10.19 | 1.68 | 0.57 |
| | | $PPP_{NG3}$ | 79.16 | 0.17 | 10.16 | 1.71 | 0.57 |
| | | $PPP_{NG2}$ | 79.02 | 0.15 | 10.03 | 1.72 | 0.58 |
| | | $PPP_{NG1}$ | 71.78 | **0.05** | **9.57** | **1.76** | **0.65** |
| | ViT | Baseline | 59.47 | *0.95* | *30.96* | *0.01* | *0.05* |
| | | NG3 | 59.45 | 0.89 | 26.40 | 0.03 | 0.11 |
| | | NG2 | 59.56 | 0.25 | 11.42 | 1.15 | 0.57 |
| | | NG1 | 53.90 | 0.02 | 6.92 | 3.29 | 0.67 |
| | | PRECODE | 59.54 | 0.21 | 10.78 | 1.39 | 0.58 |
| | | $PPP_{NG3}$ | **59.69** | 0.20 | 10.63 | 1.43 | 0.58 |
| | | $PPP_{NG2}$ | 59.44 | 0.06 | 8.01 | 2.55 | 0.65 |
| | | $PPP_{NG1}$ | *53.76* | **0.01** | **6.52** | **3.63** | **0.68** |

and our proposed approach for seminal model architectures. Covering convolutional neural networks, we consider a LeNet architecture that corresponds to the one used in [3]. For deeper networks with skip connections, we consider a ResNet-18 [46]. Lastly, given the recent success of attention-based network architectures, we also consider a Vision Transformer (ViT) [47].

We evaluated all architectures w.r.t. performance and privacy leakage as detailed in Section 4. As baseline, we used all architectures without any defense mechanism. Based on the results from Section 5.2, we excluded all mechanisms based on gradient compression due to their insufficient privacy protection and negative impact on model performance. Also NG05 caused notable reduction in model performance and was removed from further experimentation accordingly.

The results for all experiments are summarized in Table 3. A more detailed overview of all results including standard deviations and exemplary reconstruction examples can be found in the *Supplementary Material*.

Majority of the results confirm the findings made for the MLP. However, it is interesting to observe that PRECODE often offers sufficient protection against gradient leakage for most

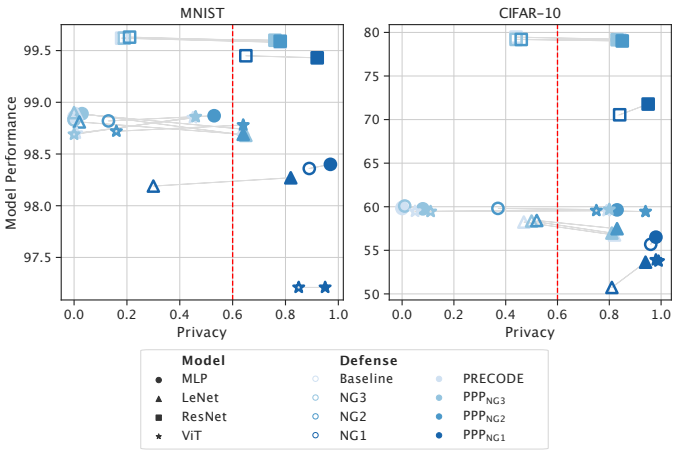


Fig. 6: **Model Performance – Privacy trade-off** for different model architectures and defense mechanisms. Model performance and privacy are displayed in terms of test accuracy and $1-\text{SSIM}$. Model architectures are differentiated by marker symbols. Color indicates the level of noise. Empty symbols display models without PRECODE/PPP whereas filled symbols display models extended by PRECODE/PPP. The red line indicates the threshold for attack success.

architectures. This is especially observed for architectures based on convolution layers, *i.e.*, LeNet and ResNet. Convolutional neural networks (CNNs) inherently offer some protection against gradient leakage due to local connectivity and parameter sharing of sliding convolutions. The ViT also uses shared parameters that are locally connected to each image patch. However, in contrast to CNNs these patches do not overlap, allowing to better reconstruct inputs to the ViT. Comparing the baseline models, the ViT offers the least architecture-inherent protection. Comparing datasets, we also observe that increased diversity of training data inherently increases protection of most architectures.

However, these mechanisms alone do not guarantee that there is sufficient protection against gradient leakage. Instead, if PRECODE does not sufficiently protect, *e.g.*, as for the ViT on MNIST, our proposed combination $PPP_{NG2}$, *i.e.*, PPP with moderate Gaussian noise with $\sigma = 10^{-2}$, offers the best performing trade-off between model performance and privacy protection.

To illustrate the trade-off between model performance and privacy for all considered models and defense methods, we aggregated the results into Figure 6. Model performance and privacy are represented as test accuracy and $1-\text{SSIM}$ respectively. An optimal model would have perfect model performance and privacy, locating itself in the top right corner of the plots. Upon extending models by PRECODE and PPP, a shift towards increased privacy can be observed for all model architectures. The red line in Figure 6 denotes the privacy threshold. Models located to the right of the threshold can be considered privacy preserving, as gradient inversion attacks result in reconstruction of training data with no more than $0.4$ SSIM on average. Lighter shades of blue, *i.e.* less perturbation, tends to have higher performance and lower privacy, which displays the already observed performance – privacy trade-off. Compared to other architectures, the model performance of LeNet decreases upon extending by PRECODE or PPP. In general, the use of PRECODE or PPP slightly decreases model performance for CNN architectures. In contrast, the performance is

slightly increased or constant for MLPs and Transformers. Similar regularizing effects when extending architectures by variational modeling were reported by [48], [49]. In addition, if large amounts of gradient perturbation (dark blue symbols in Figure 6) are required to protect from gradient leakage, PPP always increases model performance as the gradients are only partially perturbed.

## 6 Conclusion

Consistent with findings of recent work [2], [3], [4], [5], [14], [15] we observe the inherent trade-off between model performance and privacy when using gradient perturbation methods to prevent deep gradient leakage. By analyzing gradients during gradient inversion attacks we reveal how PRECODE – a privacy enhancing model extension – counters such attacks by design. We show that the privacy inducing effect of PRECODE originate from the stochastic gradients that are caused by the use of variational modeling. We derive an attack that purposefully ignores these layers' gradients during attack to disable PRECODE's privacy preserving capabilities and show that training data can be successfully reconstructed. Using PRECODE forces an attacker to omit previously usable gradient information during attack optimization, which in turn increases attack difficulty. Therefore, instead of perturbing the gradients of all layers to protect from gradient leakage, only gradients that are still usable for the attack need to be perturbed. Our proposed combination of PRECODE with Partial Perturbation, namely PPP, offers a notable increase in privacy preservation for all considered architectures while offering a better model performance trade-off. Whereas full gradient perturbation requires perturbation levels that inherently cause a drop in model performance, PPP barely impacts the model performance while achieving superior protection. Our findings are supported by systematic experiments on four seminal model architectures trained on two image classification datasets.

Whereas empirically evaluated for image classification tasks, we consider our approach to be immediately extendable to other domains such as natural language processing. As non-i.i.d. data is known to impact federated learning, we look forward to investigate its impact on PRECODE's variational bottleneck. Furthermore, we leave the comparison to other data- and model-based defense mechanisms [50], [51], [52], [53], [54], [55], [56] and adaptive perturbation techniques [11], [12] to future work. Finally, we conclude that the combination of multiple defense mechanisms is a promising research direction towards protection from gradient leakage.

## 7 Acknowledgment

We are funded by the Thuringian Ministry for Economic Affairs, Science and Digital Society (Grant: 5575/10-3).

## References

[1] P. Kairouz, H. B. McMahan, B. Avent, A. Bellet, M. Bennis, A. N. Bhagoji, K. Bonawitz, Z. Charles, G. Cormode, R. Cummings, R. G. D'Oliveira, H. Eichner, S. El Rouayheb, D. Evans, J. Gardner, Z. Garrett, A. Gascón, B. Ghazi, P. B. Gibbons, M. Gruteser, Z. Harchaoui, C. He, L. He, Z. Huo, B. Hutchinson, J. Hsu, M. Jaggi, T. Javidi, G. Joshi, M. Khodak, J. Konecní, A. Korolova, F. Koushanfar, S. Koyejo, T. Lepoint, Y. Liu, P. Mittal, M. Mohri, R. Nock, A. Özgür, R. Pagh, H. Qi, D. Ramage, R. Raskar, M. Raykova, D. Song, W. Song, S. U. Stich, Z. Sun, A. T. Suresh, F. Tramèr, P. Vepakomma, J. Wang, L. Xiong, Z. Xu, Q. Yang, F. X. Yu, H. Yu, and S. Zhao, "Advances and open problems in federated learning," *Foundations and Trends in Machine Learning*, vol. 14, no. 1-2, pp. 1–210, 2021.

[2] L. Zhu and S. Han, "Deep Leakage from Gradients," *Lecture Notes in Computer Science (including subseries Lecture Notes in Artificial Intelligence and Lecture Notes in Bioinformatics)*, vol. 12500 LNCS, no. NeurIPS, pp. 17–31, 2020.

[3] B. Zhao, K. R. Mopuri, and H. Bilen, "iDLG: Improved Deep Leakage from Gradients," pp. 1–5, 2020.

[4] W. Wei, L. Liu, M. Loper, K.-H. Chow, M. E. Gursoy, S. Truex, and Y. Wu, "A Framework for Evaluating Gradient Leakage Attacks in Federated Learning," 2020.

[5] J. Geiping, H. Bauermeister, H. Dröge, and M. Moeller, "Inverting gradients - How easy is it to break privacy in federated learning?" *Advances in Neural Information Processing Systems*, vol. 2020-Decem, no. 1, pp. 1–11, 2020.

[6] H. Yin, A. Mallya, A. Vahdat, J. M. Alvarez, J. Kautz, and P. Molchanov NVIDIA, "See Through Gradients: Image Batch Recovery via GradInversion," pp. 16 337–16 346, 2021.

[7] K. Bonawitz, V. Ivanov, B. Kreuter, A. Marcedone, H. B. McMahan, S. Patel, D. Ramage, A. Segal, and K. Seth, "Practical secure aggregation for privacy-preserving machine learning," in *Proceedings of the ACM Conference on Computer and Communications Security*, 2017, pp. 1175–1191.

[8] B. Jayaraman and D. Evans, "Evaluating differentially private machine learning in practice," *Proceedings of the 28th USENIX Security Symposium*, pp. 1895–1912, 2019.

[9] N. Papernot, S. Chien, S. Song, A. Thakurta, and U. Erlingsson, "Making the Shoe Fit: Architectures, Initializations, and Tuning for Learning with Privacy," Sep. 2019.

[10] F. Sattler, S. Wiedemann, K. R. Muller, and W. Samek, "Robust and Communication-Efficient Federated Learning from Non-i.i.d. Data," *IEEE Transactions on Neural Networks and Learning Systems*, vol. 31, no. 9, pp. 3400–3413, Sep. 2020.

[11] L. Lyu, "DP-SignSGD: When efficiency meets privacy and robustness," *ICASSP, IEEE International Conference on Acoustics, Speech and Signal Processing - Proceedings*, vol. 2021-June, pp. 3070–3074, 2021.

[12] W. Wei and L. Liu, "Gradient Leakage Attack Resilient Deep Learning," *IEEE Transactions on Information Forensics and Security*, 2021.

[13] C. Dwork and A. Roth, "The algorithmic foundations of differential privacy," *Foundations and Trends in Theoretical Computer Science*, vol. 9, no. 3-4, pp. 211–487, 2013.

[14] D. Scheliga, P. Mäder, and M. Seeland, "PRECODE - A Generic Model Extension to Prevent Deep Gradient Leakage," Aug. 2021.

[15] Y. Huang, S. Gupta, Z. Song, K. Li, and S. Arora, "Evaluating Gradient Inversion Attacks and Defenses in Federated Learning," Nov. 2021.

[16] J. Konečn, H. Brendan McMahan, F. X. Yu, A. Theertha Suresh, D. Bacon Google, and P. Richtárik, "Federated Learning: Strategies for Improving Communication Efficiency," Oct. 2016.

[17] A. G. Roy, S. Siddiqui, S. Pölsterl, N. Navab, and C. Wachinger, "BrainTorrent: A Peer-to-Peer Environment for Decentralized Federated Learning," pp. 1–9, 2019.

[18] J.-w. Lee, J. Oh, S. Lim, S.-Y. Yun, and J.-G. Lee, "TornadoAggregate: Accurate and Scalable Federated Learning via the Ring-Based Architecture," no. 2020, 2020.

[19] M. Duan, D. Liu, X. Chen, R. Liu, Y. Tan, and L. Liang, "Self-Balancing Federated Learning with Global Imbalanced Data in Mobile Systems," *IEEE Transactions on Parallel and Distributed Systems*, vol. 32, no. 1, pp. 59–71, 2021.

[20] D. C. Liu and J. Nocedal, "On the limited memory BFGS method for large scale optimization," *Mathematical Programming 1989 45:1*, vol. 45, no. 1, pp. 503–528, Aug. 1989.

[21] L. I. Rudin, S. Osher, and E. Fatemi, "Nonlinear total variation based noise removal algorithms," *Physica D: Nonlinear Phenomena*, vol. 60, no. 1-4, pp. 259–268, Nov. 1992.

[22] D. P. Kingma and J. L. Ba, "Adam: A Method for Stochastic Optimization," *3rd International Conference on Learning Representations, ICLR 2015 - Conference Track Proceedings*, Dec. 2014.

[23] Y. Wang, J. Deng, D. Guo, C. Wang, X. Meng, H. Liu, C. Ding, and S. Rajasekaran, "SAPAG: A Self-Adaptive Privacy Attack From Gradients," 2020.

[24] X. Jin, P.-Y. Chen, C.-Y. Hsu, C.-M. Yu, and T. Chen, "Catastrophic Data Leakage in Vertical Federated Learning," *Advances in Neural Information Processing Systems*, vol. 34, Dec. 2021. [Online]. Available: https://github.com/DeRafael/CAFE.

[25] J. Jeon, J. Kim, K. Lee, S. Oh, and J. Ok, "Gradient Inversion with Generative Image Prior," Oct. 2021.

[26] Z. Li, L. Wang, G. Chen, M. Shafq, and Z. Gu, "A Survey of Image Gradient Inversion Against Federated Learning," Jan. 2022. [Online].

Available: /articles/preprint/A{_}Survey{_}of{_}Image{_}Gradient{_}Inversion{_}Against{_}Federated{_}Learning/18254723/1

[27] X. Pan, M. Zhang, Y. Yan, J. Zhu, and M. Yang, "Theory-Oriented Deep Leakage from Gradients via Linear Equation Solver," pp. 1–37, 2020.

[28] J. Zhu and M. Blaschko, "R-GAP: Recursive Gradient Attack on Privacy," pp. 1–17, 2020.

[29] A. C. Yao, "PROTOCOLS FOR SECURE COMPUTATIONS." *Annual Symposium on Foundations of Computer Science - Proceedings*, pp. 160–164, 1982.

[30] C. Gentry, "Fully Homomorphic Encryption Using Ideal Lattices," *Proceedings of the Annual ACM Symposium on Theory of Computing*, pp. 169–178, 2009.

[31] L. T. Phong, Y. Aono, T. Hayashi, L. Wang, and S. Moriai, "Privacy-Preserving Deep Learning via Additively Homomorphic Encryption," *IEEE Transactions on Information Forensics and Security*, vol. 13, no. 5, pp. 1333–1345, 2018.

[32] D. Pasquini, D. Francati, and G. Ateniese, "Eluding Secure Aggregation in Federated Learning via Model Inconsistency," Nov. 2021.

[33] Y. Lin, S. Han, H. Mao, Y. Wang, and W. J. Dally, "Deep Gradient Compression: Reducing the Communication Bandwidth for Distributed Training," Dec. 2017.

[34] Y. Tsuzuku, H. Imachi, and T. Akiba, "Variance-based Gradient Compression for Efficient Distributed Deep Learning," *6th International Conference on Learning Representations, ICLR 2018 - Workshop Track Proceedings*, Feb. 2018.

[35] H. Brendan McMahan, E. Moore, D. Ramage, S. Hampson, and B. Agüera y Arcas, "Communication-efficient learning of deep networks from decentralized data," *Proceedings of the 20th International Conference on Artificial Intelligence and Statistics, AISTATS 2017*, vol. 54, 2017.

[36] H. B. McMahan, D. Ramage, K. Talwar, and L. Zhang, "Learning Differentially Private Recurrent Language Models," *6th International Conference on Learning Representations, ICLR 2018 - Conference Track Proceedings*, Oct. 2017.

[37] W. Li, F. Milletarì, D. Xu, N. Rieke, J. Hancox, W. Zhu, M. Baust, Y. Cheng, S. Ourselin, M. J. Cardoso, and A. Feng, "Privacy-Preserving Federated Brain Tumour Segmentation," *Lecture Notes in Computer Science (including subseries Lecture Notes in Artificial Intelligence and Lecture Notes in Bioinformatics)*, vol. 11861 LNCS, pp. 133–141, 2019.

[38] D. P. Kingma and M. Welling, "Auto-Encoding Variational Bayes," *2nd International Conference on Learning Representations, ICLR 2014 - Conference Track Proceedings*, Dec. 2013.

[39] L. T. Phong, Y. Aono, T. Hayashi, L. Wang, and S. Moriai, "Privacy-Preserving Deep Learning: Revisited and Enhanced," *Communications in Computer and Information Science*, vol. 719, pp. 100–110, 2017. [Online]. Available: https://link.springer.com/chapter/10.1007/978-981-10-5421-1{_}9

[40] M. Balunović, D. I. Dimitrov, R. Staab, and M. Vechev, "Bayesian Framework for Gradient Leakage," Nov. 2021.

[41] L. Deng, "The MNIST database of handwritten digit images for machine learning research," *IEEE Signal Processing Magazine*, vol. 29, no. 6, pp. 141–142, 2012.

[42] A. Krizhevsky, "Learning Multiple Layers of Features from Tiny Images," 2009.

[43] Z. Wang, A. C. Bovik, H. R. Sheikh, and E. P. Simoncelli, "Image quality assessment: From error visibility to structural similarity," *IEEE Transactions on Image Processing*, vol. 13, no. 4, pp. 600–612, Apr. 2004.

[44] R. Zhang, P. Isola, A. A. Efros, E. Shechtman, and O. Wang, "The Unreasonable Effectiveness of Deep Features as a Perceptual Metric," *Proceedings of the IEEE conference on computer vision and pattern recognition*, pp. 586–595, 2018. [Online]. Available: https://www.github.com/richzhang/PerceptualSimilarity.

[45] M. Abadi, H. B. McMahan, A. Chu, I. Mironov, L. Zhang, I. Goodfellow, and K. Talwar, "Deep learning with differential privacy," *Proceedings of the ACM Conference on Computer and Communications Security*, vol. 24-28-Octo, pp. 308–318, 2016.

[46] K. He, X. Zhang, S. Ren, and J. Sun, "Deep residual learning for image recognition," *Proceedings of the IEEE Computer Society Conference on Computer Vision and Pattern Recognition*, vol. 2016-Decem, pp. 770–778, Dec. 2016.

[47] A. Dosovitskiy, L. Beyer, A. Kolesnikov, D. Weissenborn, X. Zhai, T. Unterthiner, M. Dehghani, M. Minderer, G. Heigold, S. Gelly, J. Uszkoreit, and N. Houlsby, "An Image is Worth 16x16 Words: Transformers for Image Recognition at Scale," Oct. 2020.

[48] A. A. Alemi, I. Fischer, J. V. Dillon, and K. Murphy, "Deep variational information bottleneck," *5th International Conference on Learning Representations, ICLR 2017 - Conference Track Proceedings*, pp. 1–19, 2017.

[49] M. Hofmann and P. Mader, "Synaptic Scaling–An Artificial Neural Network Regularization Inspired by Nature," *IEEE Transactions on Neural Networks and Learning Systems*, pp. 1–15, 2021.

[50] H. Zhang, M. Cisse, Y. N. Dauphin, and D. Lopez-Paz, "mixup: Beyond Empirical Risk Minimization," *6th International Conference on Learning Representations, ICLR 2018 - Conference Track Proceedings*, Oct. 2017.

[51] W. Gao, S. Guo, T. Zhang, H. Qiu, Y. Wen, and Y. Liu, "Privacy-Preserving Collaborative Learning With Automatic Transformation Search," pp. 114–123, 2021.

[52] Y. Huang, Z. Song, K. Li, and S. Arora, "InstaHide: Instance-hiding Schemes for Private Distributed Learning," pp. 4507–4518, Nov. 2020. [Online]. Available: https://proceedings.mlr.press/v119/huang20i.html

[53] H. Lee, J. Kim, S. Ahn, R. Hussain, S. Cho, and J. Son, "Digestive neural networks: A novel defense strategy against inference attacks in federated learning," *Computers & Security*, vol. 109, p. 102378, Oct. 2021.

[54] J. Sun, A. Li, B. Wang, H. Yang, H. Li, and Y. Chen, "Soteria: Provable Defense Against Privacy Leakage in Federated Learning From Representation Perspective," pp. 9311–9319, 2021. [Online]. Available: https://github.com/jeremy313/Soteria.

[55] Y. Wu, Y. Kang, J. Luo, Y. He, and Q. Yang, "FedCG: Leverage Conditional GAN for Protecting Privacy and Maintaining Competitive Performance in Federated Learning," Nov. 2021.

[56] Q. Yang, J. Zhang, W. Hao, G. Spell, and L. Carin, "FLOP: Federated Learning on Medical Datasets using Partial Networks," *Proceedings of the ACM SIGKDD International Conference on Knowledge Discovery and Data Mining*, no. 21, pp. 3845–3853, Feb. 2021.

[57] M. S. Khine, "What Can We Learn from Gradients?" pp. 1–12, Sep. 2019.

[58] L. Fan, K. W. Ng, C. Ju, T. Zhang, C. Liu, C. S. Chan, and Q. Yang, "Rethinking Privacy Preserving Deep Learning: How to Evaluate and Thwart Privacy Attacks," *Lecture Notes in Computer Science (including subseries Lecture Notes in Artificial Intelligence and Lecture Notes in Bioinformatics)*, vol. 12500 LNCS, pp. 32–50, 2020.

**Daniel Scheliga** received his master's degree in computer science from Technische Universität Ilmenau, Ilmenau, Germany, in 2020. During the work on his thesis concerning GAN-based anomaly detection in image data, he was integrated in the Software Engineering for Safety-Critical Systems group of TU Ilmenau. Currently he is pursuing his doctoral degree on privacy enhancing methods for federated learning scenarios within the Data-intensive Systems and Visualization group of TU Ilmenau.

**Patrick Mäder** received the Diploma degree in industrial engineering and the Ph.D. degree (Hons.) in computer science from Technische Universität Ilmenau, Ilmenau, Germany, in 2003 and 2009, respectively. He was a Consultant for EXTESSY AG, Wolfsburg, Germany, a Post-Doctoral Fellow with the Institute for Systems Engineering and Automation (SEA), Johannes Kepler University Linz, Linz, Austria, Post-Doctoral Researcher with the Software and Requirements Engineering Center, DePaul University, Chicago, IL, USA, and Professor with Technische Universität Ilmenau, Ilmenau, Germany, where he has been the Endowed Chair on Software Engineering for Safety-Critical Systems. He is currently Professor with Technische Universität Ilmenau, Ilmenau, Germany, heading the Chair on Data-intensive Systems and Visualization. His research interests include machine learning, software engineering, and safety engineering.

**Marco Seeland** received the Master's degree in Technical Physics from Technische Universität Ilmenau, Ilmenau, Germany, in 2012. After receiving the Ph.D. degree in Physics in 2015, he fulfilled a long-standing passion and started researching in the field of computer science. As a member of the Data-intensive Systems and Visualization group of TU Ilmenau, his main research interests are development and scaling of neural networks for computer vision and pattern recognition in ecological bioinformatics.

# Supplementary Material

## Defending against analytical attacks

Since the input to any fully connected layer in a neural network can be analytically reconstructed [5], [39], Multi Layer Perceptrons (MLP) are – even with the protection of PRECODE – vulnerable to gradient inversion [40]. Given the gradients of the loss $\mathcal{L}$ with regards to the weights $\Theta_W^{(l)}$ and the bias $\Theta_b^{(l)}$ of a fully connected layer $l$, the input $x$ to that layer can be perfectly reconstructed by calculating:

$$x^T = \left( \frac{d\mathcal{L}}{d\Theta_{b_i}^{(l)}} \right)^{-1} \cdot \frac{d\mathcal{L}}{d\Theta_{W_i}^{(l)}}, \tag{5}$$

where $i$ refers to the line of $\Theta_W^{(l)}$ and $\Theta_b^{(l)}$. Further analysis of analytical reconstruction techniques is presented in [57], [58]. Note that $\frac{d\mathcal{L}}{d\Theta_b^{(l)}}$ requires to have at least one non-zero entry, which experimentally seems to always be the case [40].

However, we propose to remove the bias weights from all fully connected layers to entirely mitigate this problem. We empirically analyzed the impact of this removal on the performance of models in a federated training scenario as described in the experimental setup. As model architecture for this experiment we naturally consider a MLP which is composed of four fully connected layers with $1024$ neurons, batch normalization and ReLU activation. The number of neurons in the last fully connected output layer with softmax activation is equal to the number of classes within a dataset. The model is trained with and without PRECODE and both with enabled and disabled biases for the CIFAR-10 dataset.

TABLE 4: Test accuracies for a MLP trained in a federated manner with and without bias weights and PRECODE.

| Accuracy [%] ↑ | Bias | No Bias |
|---|---|---|
| Baseline | 59.91 | 59.98 |
| PRECODE | 59.80 | 59.67 |

Table 4 summarizes the test accuracies for the MLP with/without bias and with/without PRECODE. As removing the bias weights from the models only marginally affects model performance, it poses a simple yet effective defense against analytical attack. Furthermore, we did not observe any effects on the success of iterative gradient inversion attacks when biases were disabled.

## Increasing Attack Costs

Table 5 compares the mean number of iterations the attacker performed before termination. While PRECODE did not preserve privacy under our targeted attack as discussed in Section 5.1 of the main paper, the computational effort of the attacker notably increases.

TABLE 5: Mean number of iterations required for image reconstruction for a MLP trained on MNIST and CIFAR-10. The gradients are attacked without defense, with PRECODE and with PRECODE using our proposed targeted attack indicated by $^*$.

| Dataset | Metric / Defense | Needed Iterations |
|---|---|---|
| MNIST | Baseline | *1666* |
| | PRECODE | 7210 |
| | PRECODE* | **7897** |
| CIFAR-10 | Baseline | *2869* |
| | PRECODE | 7738 |
| | PRECODE* | **9366** |

## All Results

Table 6 summarizes the experimental results for all considered model architectures for the MNIST and CIFAR-10 datasets. Figures 7-14 visualize more reconstruction examples for the considered defenses.

TABLE 6: Mean and standard deviation of model performance and privacy metrics for a MLP, LeNet, ResNet and Vision Transformer (ViT) trained on MNIST and CIFAR-10. The gradients are attacked for different defense mechanisms. When PRECODE or PPP is used, our proposed targeted attack is applied. Arrows indicate direction of improvement. Bold and italic formatting highlight best and worst results respectively.

| Dataset | Model | Metric / Defense | Accuracy [%] ↑ | SSIM ↓ | PSNR ↓ | MSE ↑ | LPIPS ↑ |
|---|---|---|---|---|---|---|---|
| MNIST | MLP | Baseline | 98.83 (±0.03) | *1.00 (±0.00)* | *60.09 (±3.51)* | *0.00 (±0.00)* | *0.00 (±0.00)* |
| | | NG3 | 98.83 (±0.03) | *1.00 (±0.00)* | 42.41 (±2.01) | *0.00 (±0.00)* | 0.01 (±0.00) |
| | | NG2 | 98.82 (±0.03) | 0.87 (±0.07) | 22.29 (±1.03) | 0.06 (±0.02) | 0.20 (±0.05) |
| | | NG1 | 98.36 (±0.05) | 0.11 (±0.05) | 7.43 (±0.39) | 1.91 (±0.17) | 0.67 (±0.02) |
| | | NG05 | 93.32 (±0.09) | 0.02 (±0.04) | **6.02 (±0.30)** | **2.64 (±0.18)** | **0.69 (±0.02)** |
| | | GC90 | 95.02 (±1.63) | 0.94 (±0.04) | 27.57 (±1.06) | 0.02 (±0.01) | 0.11 (±0.03) |
| | | GC99 | *64.93 (±16.30)* | 0.72 (±0.06) | 15.98 (±1.08) | 0.30 (±0.11) | 0.35 (±0.04) |
| | | PRECODE | 98.86 (±0.01) | *1.00 (±0.00)* | 48.02 (±5.41) | *0.00 (±0.00)* | *0.00 (±0.01)* |
| | | $PPP_{NG3}$ | **98.89 (±0.04)** | 0.97 (±0.02) | 32.32 (±2.01) | 0.01 (±0.00) | 0.05 (±0.02) |
| | | $PPP_{NG2}$ | 98.87 (±0.03) | 0.47 (±0.11) | 12.30 (±0.69) | 0.61 (±0.10) | 0.56 (±0.04) |
| | | $PPP_{NG1}$ | 98.40 (±0.10) | 0.03 (±0.04) | 7.20 (±0.43) | 2.01 (±0.20) | 0.68 (±0.02) |
| | | $PPP_{NG05}$ | 95.36 (±0.27) | **0.01 (±0.04)** | 6.92 (±0.42) | 2.15 (±0.21) | 0.68 (±0.02) |
| | | $PPP_{GC90}$ | 98.79 (±0.12) | 0.94 (±0.04) | 27.01 (±1.09) | 0.02 (±0.01) | 0.12 (±0.03) |
| | | $PPP_{GC99}$ | 88.90 (±4.01) | 0.78 (±0.08) | 17.24 (±1.01) | 0.20 (±0.05) | 0.35 (±0.04) |
| | LeNet | Baseline | 98.89 (±0.11) | 0.99 (±0.00) | 34.47 (±2.62) | *0.00 (±0.00)* | 0.01 (±0.01) |
| | | NG3 | **98.90 (±0.12)** | *1.00 (±0.00)* | *50.05 (±3.87)* | *0.00 (±0.00)* | *0.00 (±0.00)* |
| | | NG2 | 98.81 (±0.11) | 0.98 (±0.03) | 33.38 (±3.12) | 0.01 (±0.03) | 0.04 (±0.05) |
| | | NG1 | *98.19 (±0.10)* | 0.70 (±0.17) | 14.18 (±2.45) | 0.51 (±0.58) | 0.39 (±0.10) |
| | | PRECODE | 98.74 (±0.07) | 0.36 (±0.09) | 8.64 (±1.06) | 1.48 (±0.36) | 0.59 (±0.04) |
| | | $PPP_{NG3}$ | 98.68 (±0.03) | 0.35 (±0.11) | 8.57 (±1.41) | 1.54 (±0.48) | 0.59 (±0.05) |
| | | $PPP_{NG2}$ | 98.69 (±0.09) | 0.36 (±0.10) | 8.67 (±1.31) | 1.50 (±0.46) | 0.59 (±0.04) |
| | | $PPP_{NG1}$ | 98.27 (±0.05) | **0.18 (±0.07)** | **6.37 (±0.77)** | **2.46 (±0.43)** | **0.66 (±0.03)** |
| | ResNet | Baseline | 99.62 (±0.02) | *0.82 (±0.10)* | *18.24 (±2.74)* | *0.19 (±0.14)* | *0.23 (±0.08)* |
| | | NG3 | 99.62 (±0.01) | 0.81 (±0.12) | 18.06 (±2.72) | 0.20 (±0.16) | *0.23 (±0.09)* |
| | | NG2 | **99.63 (±0.01)** | 0.79 (±0.12) | 17.55 (±2.54) | 0.22 (±0.16) | 0.25 (±0.08) |
| | | NG1 | 99.45 (±0.03) | 0.35 (±0.10) | 11.17 (±1.31) | 0.84 (±0.27) | 0.50 (±0.04) |
| | | PRECODE | 99.58 (±0.02) | 0.22 (±0.15) | **7.40 (±2.41)** | **2.16 (±0.90)** | 0.57 (±0.07) |
| | | $PPP_{NG3}$ | 99.60 (±0.04) | 0.24 (±0.16) | 7.58 (±2.51) | 2.10 (±0.92) | 0.57 (±0.07) |
| | | $PPP_{NG2}$ | 99.59 (±0.01) | 0.22 (±0.13) | 7.42 (±2.05) | 2.09 (±0.78) | **0.58 (±0.06)** |
| | | $PPP_{NG1}$ | *99.43 (±0.06)* | **0.08 (±0.04)** | 8.01 (±1.21) | 1.73 (±0.47) | **0.58 (±0.04)** |
| | ViT | Baseline | 98.70 (±0.03) | 0.99 (±0.01) | 33.35 (±2.47) | 0.01 (±0.00) | 0.01 (±0.01) |
| | | NG3 | 98.69 (±0.05) | *1.00 (±0.00)* | *39.73 (±2.46)* | *0.00 (±0.00)* | *0.00 (±0.00)* |
| | | NG2 | 98.72 (±0.11) | 0.84 (±0.05) | 20.55 (±2.14) | 0.11 (±0.06) | 0.16 (±0.03) |
| | | NG1 | *97.21 (±0.15)* | 0.15 (±0.05) | 8.93 (±1.19) | 1.40 (±0.40) | 0.56 (±0.04) |
| | | PRECODE | 98.85 (±0.07) | 0.55 (±0.08) | 14.00 (±1.72) | 0.45 (±0.18) | 0.35 (±0.05) |
| | | $PPP_{NG3}$ | **98.86 (±0.03)** | 0.54 (±0.08) | 13.93 (±1.71) | 0.46 (±0.17) | 0.35 (±0.04) |
| | | $PPP_{NG2}$ | 98.78 (±0.09) | 0.36 (±0.07) | 11.40 (±1.37) | 0.80 (±0.25) | 0.46 (±0.04) |
| | | $PPP_{NG1}$ | *97.21 (±0.13)* | **0.05 (±0.04)** | **7.18 (±0.77)** | **2.05 (±0.36)** | **0.63 (±0.03)** |
| CIFAR-10 | MLP | Baseline | 59.91 (±0.09) | *1.00 (±0.00)* | *59.50 (±5.80)* | *0.00 (±0.00)* | *0.00 (±0.00)* |
| | | NG3 | **60.08 (±0.11)** | 0.99 (±0.01) | 38.65 (±1.77) | *0.00 (±0.00)* | 0.01 (±0.01) |
| | | NG2 | 59.81 (±0.17) | 0.63 (±0.11) | 18.73 (±1.41) | 0.16 (±0.03) | 0.32 (±0.09) |
| | | NG1 | 55.69 (±0.19) | 0.04 (±0.02) | 8.43 (±0.63) | 2.31 (±0.40) | **0.67 (±0.05)** |
| | | NG05 | *25.55 (±1.21)* | **0.01 (±0.01)** | **7.80 (±0.63)** | **2.69 (±0.47)** | **0.67 (±0.05)** |
| | | GC90 | 55.31 (±2.22) | 0.87 (±0.08) | 23.52 (±2.70) | 0.06 (±0.04) | 0.11 (±0.06) |
| | | GC99 | 42.14 (±1.35) | 0.43 (±0.12) | 14.45 (±2.37) | 0.62 (±0.36) | 0.40 (±0.10) |
| | | PRECODE | 59.80 (±0.17) | *1.00 (±0.01)* | 49.52 (±6.46) | *0.00 (±0.00)* | *0.00 (±0.00)* |
| | | $PPP_{NG3}$ | 59.76 (±0.11) | 0.92 (±0.05) | 28.26 (±2.20) | 0.02 (±0.01) | 0.06 (±0.05) |
| | | $PPP_{NG2}$ | 59.64 (±0.05) | 0.17 (±0.07) | 11.39 (±0.70) | 1.12 (±0.16) | 0.60 (±0.06) |
| | | $PPP_{NG1}$ | 56.51 (±0.34) | 0.02 (±0.01) | 8.57 (±0.74) | 2.23 (±0.46) | **0.67 (±0.05)** |
| | | $PPP_{NG05}$ | 48.99 (±0.21) | **0.01 (±0.01)** | 8.44 (±0.76) | 2.31 (±0.49) | **0.67 (±0.05)** |
| | | $PPP_{GC90}$ | 50.92 (±8.25) | 0.87 (±0.07) | 23.73 (±2.35) | 0.06 (±0.03) | 0.11 (±0.07) |
| | | $PPP_{GC99}$ | 38.02 (±5.42) | 0.47 (±0.13) | 15.85 (±1.92) | 0.40 (±0.23) | 0.40 (±0.10) |
| | LeNet | Baseline | 58.24 (±0.69) | *0.53 (±0.16)* | *15.61 (±2.45)* | *0.47 (±0.25)* | *0.42 (±0.12)* |
| | | NG3 | 58.36 (±0.72) | 0.50 (±0.19) | 15.14 (±3.10) | 0.62 (±0.66) | 0.44 (±0.14) |
| | | NG2 | **58.42 (±0.42)** | 0.48 (±0.19) | 14.87 (±3.05) | 0.69 (±0.87) | 0.44 (±0.12) |
| | | NG1 | *50.74 (±0.69)* | 0.19 (±0.07) | 9.55 (±0.99) | 1.85 (±0.62) | 0.61 (±0.07) |
| | | PRECODE | 56.76 (±0.45) | 0.18 (±0.07) | 9.63 (±0.62) | 1.76 (±0.26) | 0.61 (±0.07) |
| | | $PPP_{NG3}$ | 56.98 (±0.20) | 0.19 (±0.06) | 9.67 (±0.57) | 1.75 (±0.26) | 0.61 (±0.06) |
| | | $PPP_{NG2}$ | 57.48 (±0.38) | 0.17 (±0.07) | 9.42 (±0.79) | 1.87 (±0.38) | 0.61 (±0.07) |
| | | $PPP_{NG1}$ | 53.64 (±0.18) | **0.06 (±0.03)** | **7.74 (±0.51)** | **2.74 (±0.38)** | **0.66 (±0.06)** |
| | ResNet | Baseline | **79.46 (±0.06)** | *0.56 (±0.14)* | *16.27 (±1.98)* | 0.35 (±0.19) | *0.39 (±0.10)* |
| | | NG3 | 79.20 (±0.26) | *0.56 (±0.12)* | 16.19 (±1.70) | *0.34 (±0.17)* | *0.39 (±0.09)* |
| | | NG2 | 79.19 (±0.24) | 0.54 (±0.12) | 15.95 (±1.73) | 0.36 (±0.18) | 0.40 (±0.09) |
| | | NG1 | *70.55 (±0.20)* | 0.16 (±0.07) | 11.71 (±0.91) | 1.03 (±0.25) | 0.58 (±0.06) |
| | | PRECODE | 79.21 (±0.16) | 0.16 (±0.10) | 10.19 (±2.21) | 1.68 (±0.75) | 0.57 (±0.08) |
| | | $PPP_{NG3}$ | 79.16 (±0.04) | 0.17 (±0.12) | 10.16 (±2.27) | 1.71 (±0.79) | 0.57 (±0.08) |
| | | $PPP_{NG2}$ | 79.02 (±0.15) | 0.15 (±0.09) | 10.03 (±1.97) | 1.72 (±0.74) | 0.58 (±0.08) |
| | | $PPP_{NG1}$ | 71.78 (±0.24) | **0.05 (±0.03)** | **9.57 (±0.91)** | **1.76 (±0.45)** | **0.65 (±0.06)** |
| | ViT | Baseline | 59.47 (±0.25) | *0.95 (±0.05)* | *30.96 (±2.81)* | *0.01 (±0.00)* | *0.05 (±0.05)* |
| | | NG3 | 59.45 (±0.28) | 0.89 (±0.07) | 26.40 (±2.06) | 0.03 (±0.01) | 0.11 (±0.07) |
| | | NG2 | 59.56 (±0.53) | 0.25 (±0.08) | 11.42 (±0.60) | 1.15 (±0.14) | 0.57 (±0.07) |
| | | NG1 | 53.90 (±0.49) | 0.02 (±0.01) | 6.92 (±0.43) | 3.29 (±0.36) | 0.67 (±0.06) |
| | | PRECODE | 59.54 (±0.25) | 0.21 (±0.10) | 10.78 (±1.38) | 1.39 (±0.43) | 0.58 (±0.08) |
| | | $PPP_{NG3}$ | **59.69 (±0.49)** | 0.20 (±0.09) | 10.63 (±1.32) | 1.43 (±0.41) | 0.58 (±0.08) |
| | | $PPP_{NG2}$ | 59.44 (±0.15) | 0.06 (±0.03) | 8.01 (±0.45) | 2.55 (±0.28) | 0.65 (±0.06) |
| | | $PPP_{NG1}$ | *53.76 (±0.60)* | **0.01 (±0.01)** | **6.52 (±0.45)** | **3.63 (±0.43)** | **0.68 (±0.05)** |

Fig. 7: **Example reconstructions** for the MLP architecture with different defenses on the MNIST dataset.

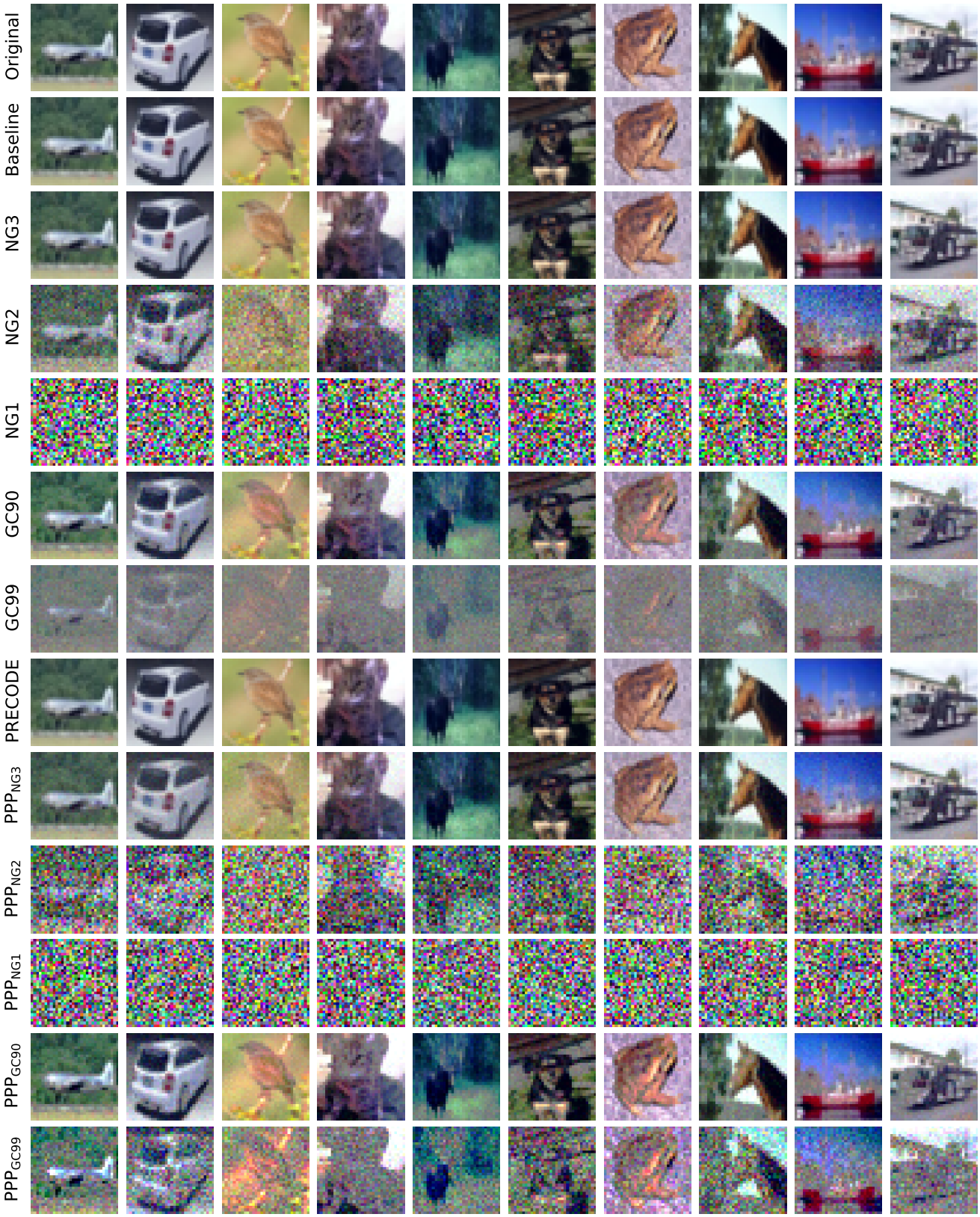


Fig. 8: **Example reconstructions** for the MLP architecture with different defenses on the CIFAR-10 datasets.

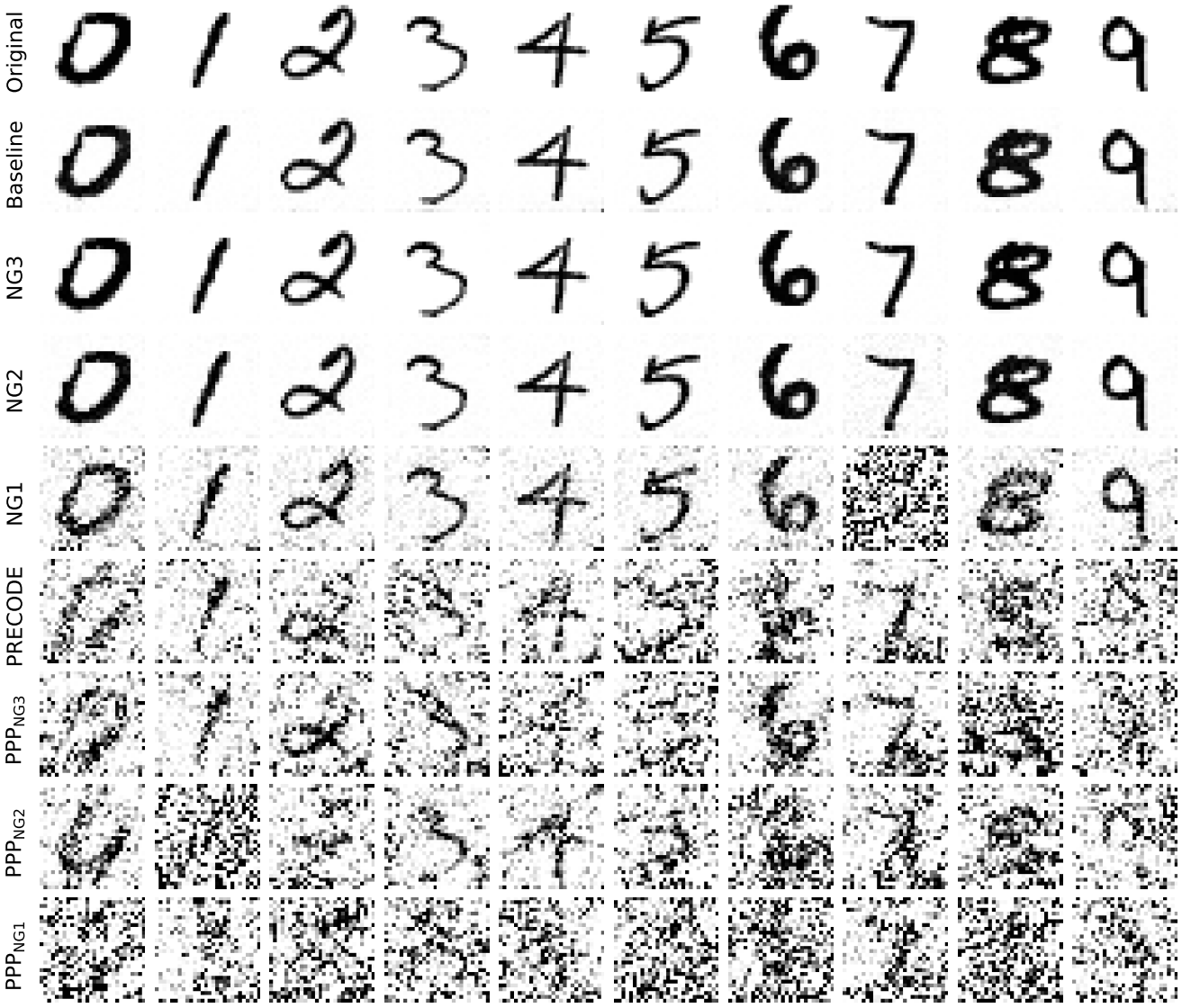


Fig. 9: **Example reconstructions** for the LeNet architecture with different defenses on the MNIST dataset.

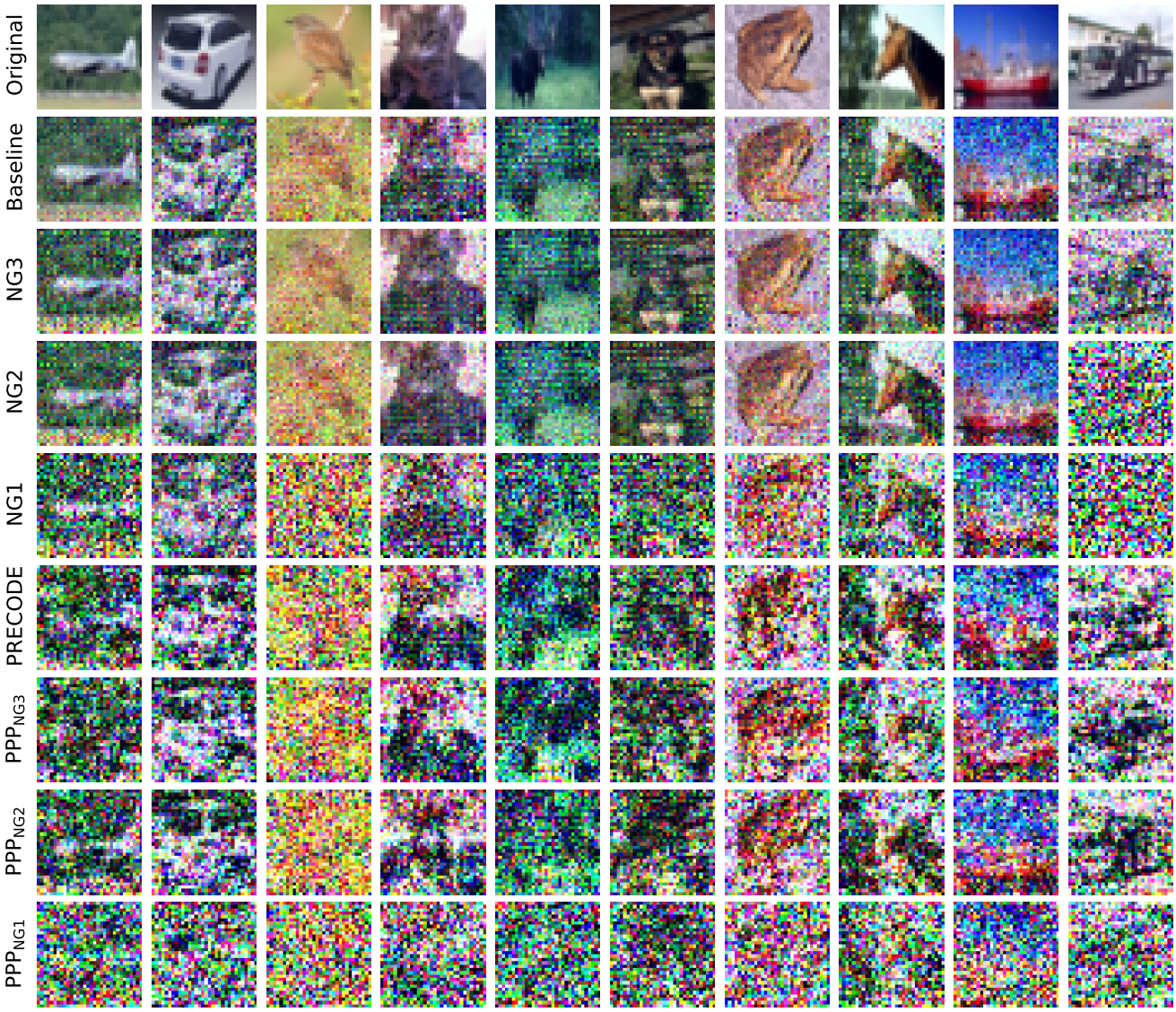


Fig. 10: **Example reconstructions** for the LeNet architecture with different defenses on the CIFAR-10 dataset.

Fig. 11: **Example reconstructions** for the ResNet architecture with different defenses on the MNIST dataset.

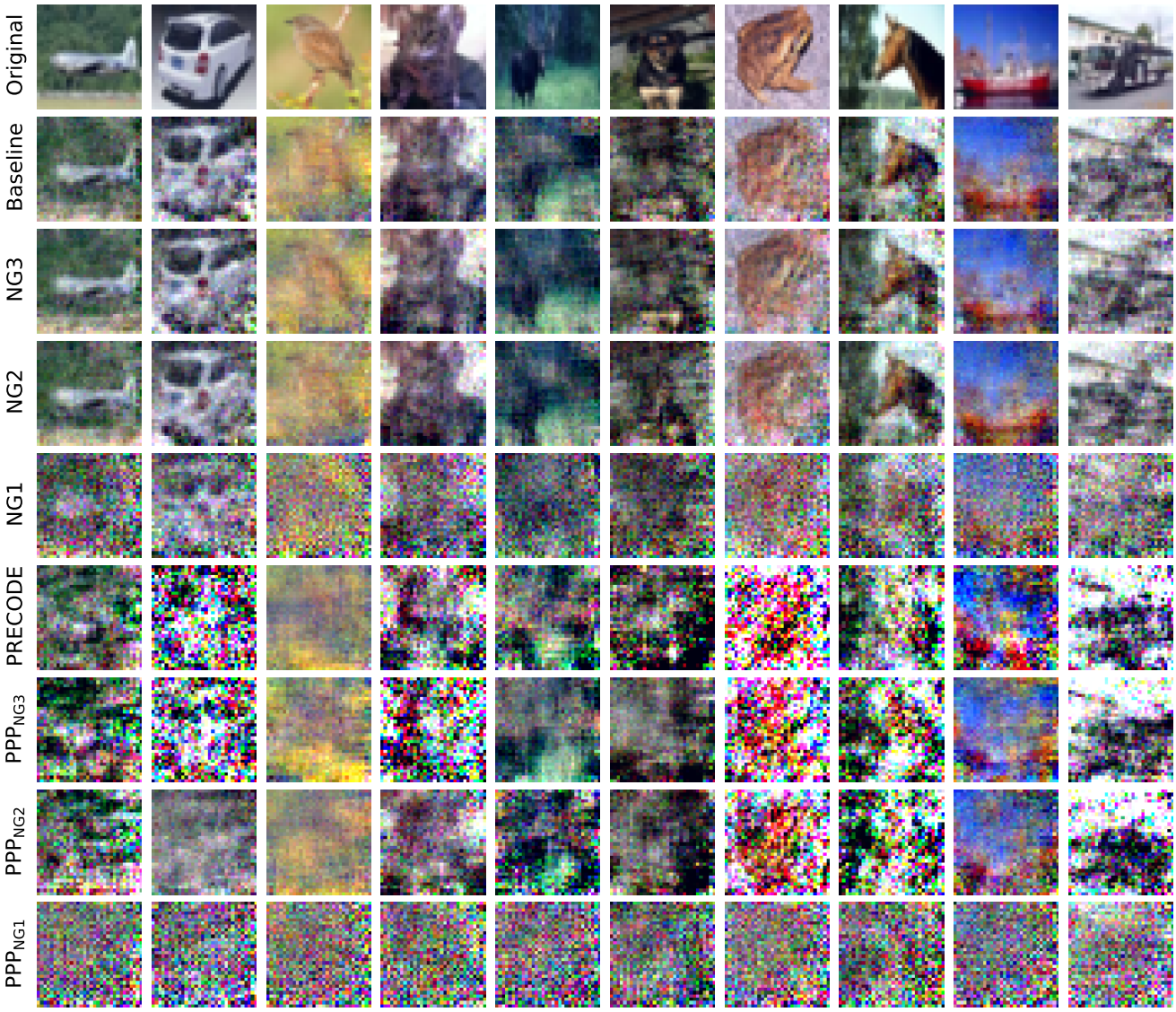


Fig. 12: **Example reconstructions** for the ResNet architecture with different defenses on the CIFAR-10 dataset.

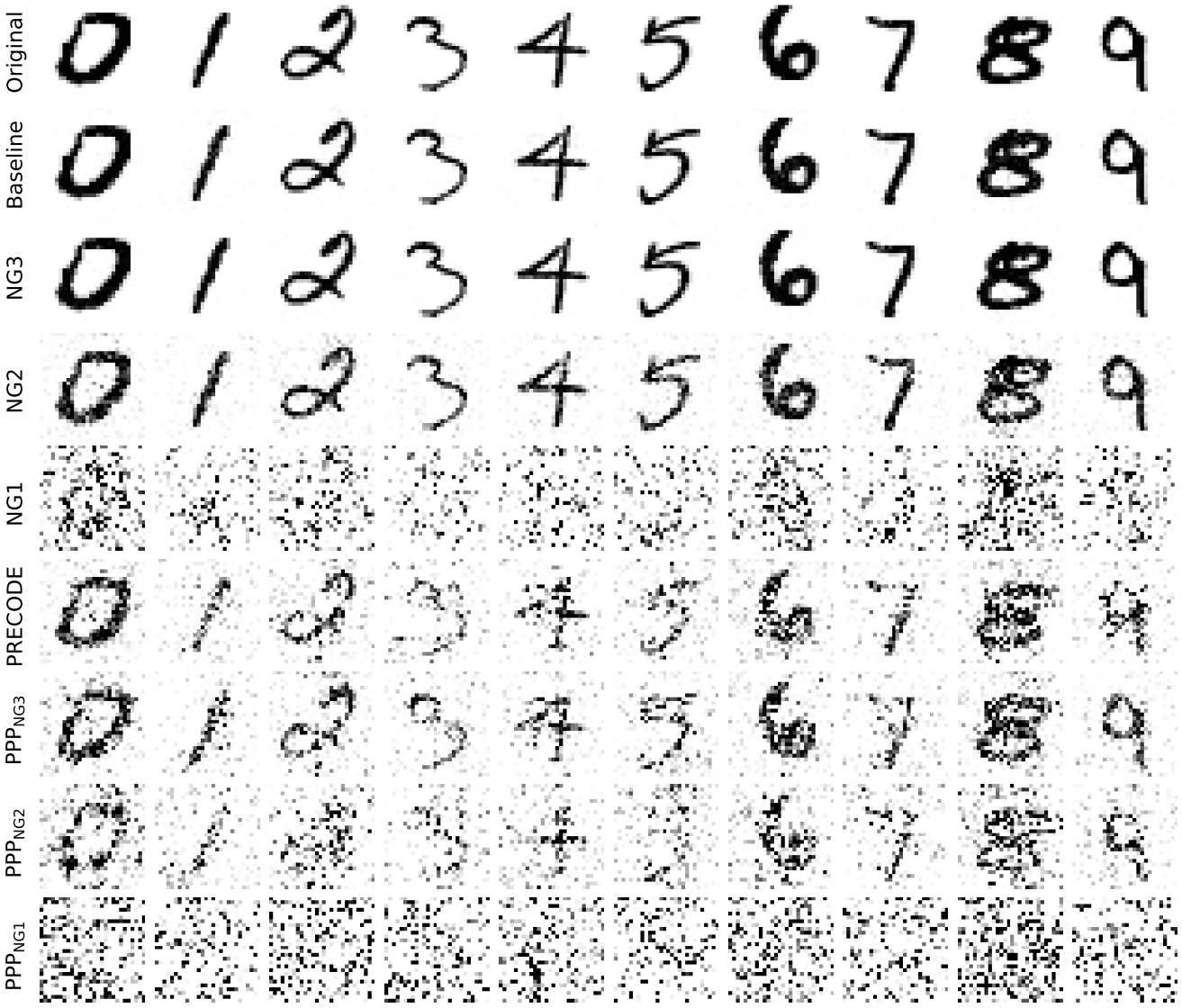


Fig. 13: **Example reconstructions** for the ViT architecture with different defenses on the MNIST dataset.

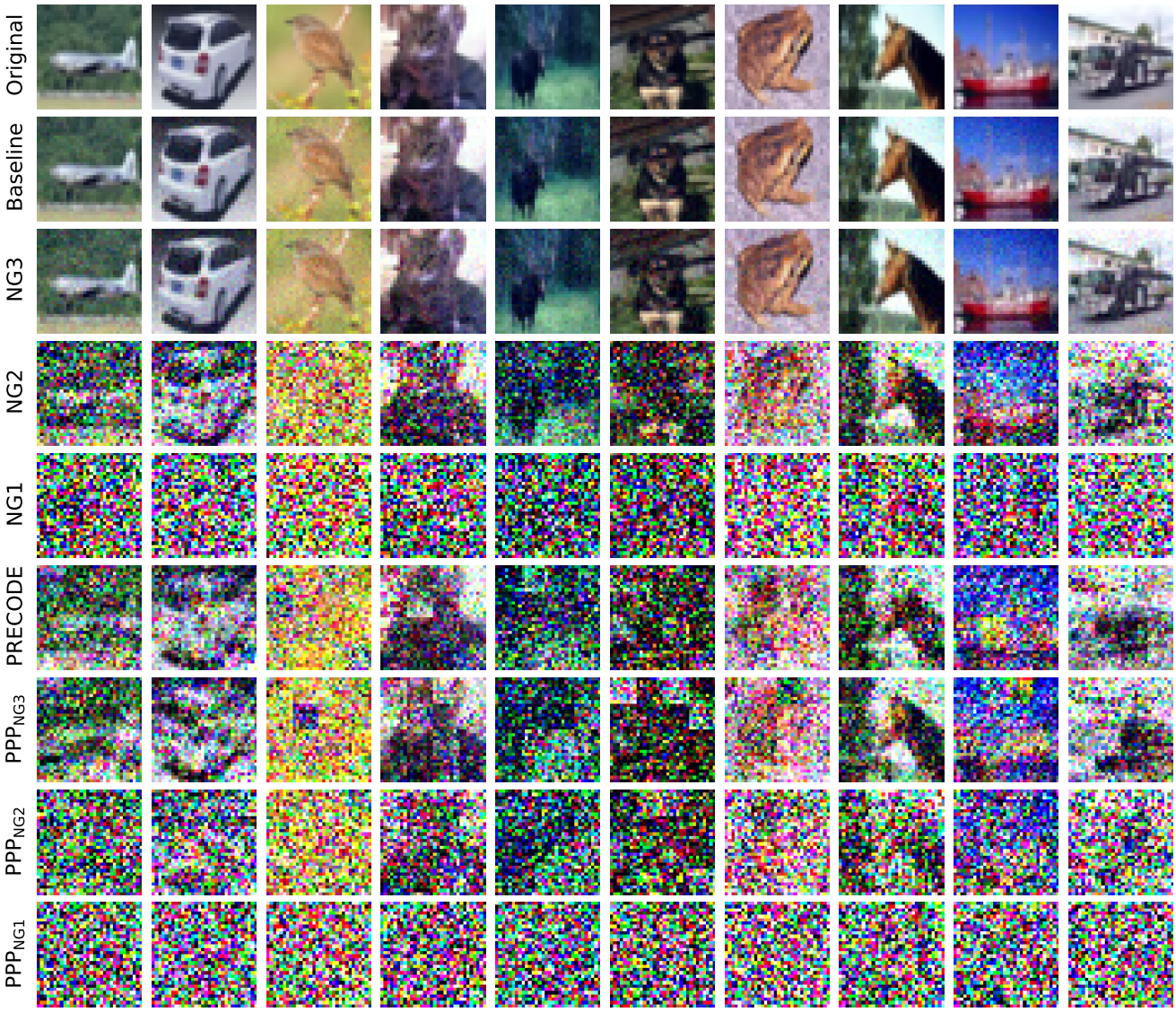


Fig. 14: **Example reconstructions** for the ViT architecture with different defenses on the CIFAR-10 dataset.